Performance measures for targeted energy transfer and resonance capture cascading in nonlinear energy sinks

Kevin Dekemele, Robin De Keyser & Mia Loccufier

Nonlinear Dynamics
An International Journal of Nonlinear Dynamics and Chaos in Engineering Systems

ISSN 0924-090X

Nonlinear Dyn
DOI 10.1007/s11071-018-4190-5

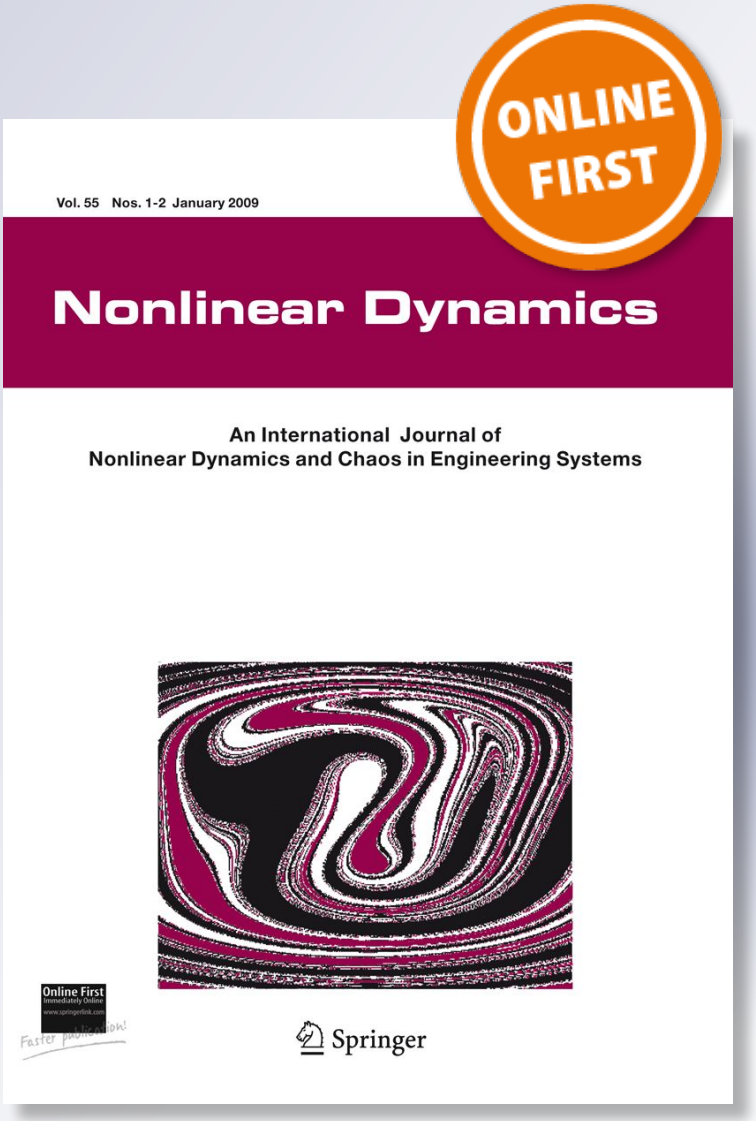

Springer

Nonlinear Dyn
https://doi.org/10.1007/s11071-018-4190-5

ORIGINAL PAPER

Performance measures for targeted energy transfer and resonance capture cascading in nonlinear energy sinks

Kevin Dekemele · **Robin De Keyser** · **Mia Loccufier**

Received: 20 October 2017 / Accepted: 4 March 2018

Abstract In vibrating mechanical systems, the targeted energy transfer mechanism (TET) of nonlinear energy sinks (NES) is employed as an alternative to linear tuned mass dampers (TMD) as passive vibrations absorbers for transient vibrations. The major advantages a NES has over a linear TMD are (1) an increased robustness to detuning and (2) the ability to dissipate multiple frequencies with only a single NES through so-called resonance capture cascading (RCC). The performance, especially the speed, of TET and RCC has rarely been a topic of research. In this research, algebraic performance measures for the speed of both TET and RCC are derived, called the pumping time and the cascading time, respectively. It shows that cascading time can be seen as a sum of single-mode pumping times, by introducing a novel modal decomposition. The strength of both measures is that they do not require numerical simulations, allowing easy optimization of the NES. The influence of different nonlinearities on the TET and RCC performance is investigated. Actual numerical simulations presented in the study validate the merit of both the pumping time and cascading time.

K. Dekemele (✉) · R. De Keyser · M. Loccufier
Department of Electrical Energy, Metals, Mechanical Construction and Systems, Ghent university, Tech Lane Ghent Science Park - Campus A, Technologiepark 914, 9052 Ghent, Belgium
e-mail: kevin.dekemele@ugent.be

Published online: 12 March 2018

Keywords Passive vibration control · Nonlinear energy sink · Targeted energy transfer · Resonance capture cascade

1 Introduction

Excessive vibrations in mechanical structures not only lead to reduced structural integrity, but also are detrimental for sensitive equipment or people. While vibrations can be counteracted with active feedback loops, often it is desired that these excessive vibrations are mitigated by passive means. In civil engineering, the vibration energy in a structure can be of such magnitude that active means would require massive amounts of energy. In aerospace sensitive equipment, cargo and people should be protected even in case of a power failure. Passive vibration absorption is often realized by local addition of a linear mass–spring–damper system, called a *tuned mass damper* (TMD). With the addition of a well-designed TMD, the vibration energy will be transferred from main mechanical structure to the TMD, where the energy is dissipated by the linear damper. Typically, for a linear TMD to perform well, the natural frequency of the added TMD is designed to be equal to the frequency of the main system's vibration, often one of the modal frequencies of this mechanical system. A single linear TMD is only capable of reducing the vibrations of a single frequency significantly. This inherent property is its main drawback. The frequency of vibrations of a mechanical system not

only can change due to different loading conditions or changes to the system itself (so-called detuning), but can consist of several dominant frequencies, a combination of the mechanical systems modal frequencies. To tackle these problems, so-called *nonlinear energy sinks* (NES) are employed, which are TMDs where the connecting stiffness is nonlinear. Because of this nonlinear stiffness, the TMD does not have a preferential (natural) frequency. As a consequence, not only is the performance of the NES more robust to detuning, a single NES is capable of absorbing multiple frequencies [1,2].

The mechanism of vibration absorption in the NES is dubbed *targeted energy transfer* (TET). It is defined as a sudden one-way irreversible transfer of energy from source (mechanical system) to a donor (NES) [1]. In the previous research, typically a numerical example of a low (often one)-dimensional main system and a connecting NES with a cubic nonlinearity and fixed coefficient is investigated thoroughly for qualitative aspects [1–6]. For transient vibrations, a threshold is observed for the initial conditions on the main mechanical system. Below this threshold, vibration absorption by the NES is very slow. Once this threshold is reached, TET occurs and vibrations are dissipated swiftly. The performance decreases again for initial condition way beyond the threshold. This sudden change of behavior is caused by an underlying bifurcation, typically found in nonlinear dynamics. Also, the occurrence of *internal resonances* is observed, where both the absorber and NES vibrate with a different frequency. Although this behavior is remarkable, it only has significant effect on the TET dynamics for certain specific main systems, where the modal frequencies either are indistinct or are commensurable, i.e., their ratio is rational number. In [5] a 3:1 internal resonance is considered by deliberately choosing a linear main system of which the eigenfrequencies have a 3:1 ratio, while in [7], two identical linear oscillators are weakly coupled, creating closely spaced eigenfrequencies. For other main systems, the frequency-energy dependence can induce internal resonance, as the increase in excitation or energy level can make the frequencies of the nonlinear modes commensurable in a small energy band [1]. The range of excitation level or initial conditions where this happens is so small that the internal resonance rarely occurs. Also, it is not associated with a strong energy transfer for the systems considered here, illustrated in numerical simulations in [1,8].

More application-oriented research expanded this threshold on the initial condition to a more general parameter threshold, independent of the numerical values of the parameters [9–11], allowing to tune the nonlinear coefficient, regardless of the numerical values of the initial condition or parameters of the main system.

The performance in terms of speed of TET is rarely assessed, while this is critical from a vibrations mitigating point of view. Usually, numerical simulation is performed, and the fraction of the total energy that is transferred during TET is used as a performance measure. This does not tell anything about the speed of the TET and requires a new numerical simulation for each parameter variation [1,12–14]. Nyugen [10] was the first to define measure of speed for the TET for undamped main systems, the so-called *pumping time* for NES attached to a single-mode vibrating systems. He showed that TET is most optimal when the initial conditions are equal to the threshold, and thus the NES nonlinearity should be tuned to ensure this optimal TET. Only a cubic nonlinearity was considered. Lin [6] expanded a similar measure for nonlinearities of power 5 and 7, yet focused only on a few numerical examples and did not consider the optimal performance at all. A powerful aspect of Nyugen's pumping time is that it is an algebraic expression depending on the parameters of the mechanical systems and NES, as well as the initial conditions. Because of this, the pumping time is calculated without the need of a numerical simulation, such that the influence of certain parameters can be easily assessed.

In the research, the idea of the pumping time is utilized to its full potential, it is extended for damped main systems and for stiffnesses which posses not only a uneven power, but also a small, both positive or negative linear part. This allows us to easily see the effect without performing any numerical simulation. It will be observed that for a single-mode vibrating mechanical system, a small positive linear part will expedite TET, while a power larger than three and negative linear impedes TET.

A major advantage a NES has over a linear TMD is the capability to dissipate multiple frequencies for transient vibrations, [15]. The mechanism of multi-frequency vibration absorption in a single NES is called resonance capture cascading (RCC), where the modal frequencies of the mechanical system are dissipated *sequentially* (hence cascaded) from higher to lower modal frequencies. This sequential nature is best

observed in the NES, which initially vibrates with a single modal frequency, even though the mechanical system vibrates with multiple modes. If enough energy of this initial mode has been dissipated, the NES will start to vibrate with the modal frequency just below the initial mode. This continues until all modes have been dissipated. The capability of RCC, just as the increased robustness to detuning of the mains system, stems from lack of 'natural' frequency of the NES, so that it can vibrate vigorously with any of the modal frequencies. Research on RCC has been given similar treatment as single-mode TET, with focus on global dynamics, internal resonances, and thorough discussion and observation of numerical examples [1,2,16]. A more recent study investigated a NES attached to a two degree-of-freedom main system [14], but only considered single-mode vibrations, despite the ability of the NES to engage in RCC with the two modal frequencies.

In this research, a more application point of view is taken for RCC. First, a tuning procedure for RCC is proposed, in which the initial mode of the cascade can be chosen. Second, the pumping time is extended to a so-called *cascading time*, by decomposing the mechanical system into its modal initial conditions. Of each modal initial condition a pumping time can be calculated, with the sum equaling the cascading time. Just as the pumping time, the cascading time is determined without any numerical simulations, which allows us to asses many different NES configurations quickly.

The effect of additional linear stiffness and high powers of the NES on cascading time is more nuanced than the single-mode pumping time. Under certain conditions, a positive linear part will impede the cascading time, and a negative linear part and power higher than three will actually expedites the cascading, the opposite effect it had on the pumping time.

The paper is structured as follows: first the dynamics of the mechanical system and the coupling with the NES are derived, by assuming a single-mode vibration. On these coupled nonlinear dynamics, the semi-analytic techniques, perturbation series and two-timing are applied. A static expression is found which describes the dynamics on a slow time scale, the so-called slow invariant manifold (SIM). With this curve, the performance measures energy dissipation and pumping time are defined, the latter for undamped main systems. Next, the pumping time is calculated for a numerical example, and simulations are performed to observe how the algebraic performance measure pumping time appears in simulation of the actual, fast dynamics. Next, for multi-modal vibrations, the cascading time is derived by decoupling the initial conditions of the mechanical system, and then, simulations are performed to validate algebraic cascading time as well. Finally, it is investigated if the performance can still be assessed if a main system with slight nonlinearity or damping is considered.

2 List of symbols

Symbol	Name
α_p	Nonlinear coefficient of NES stiffness per m_{na}
A_{TET}	Amplitude reduction during TET
ε	Ratio of m_{na} and m_e.
$e_i(\ell)$	ℓ'th component of eigenvector of mode i
E	Eigenvector matrix of linear main system
E_0	Energy in center of mass
E_{na}	Energy in relative NES movement
E_{TET}	Energy dissipation during TET
κ	Dimensionless linear stiffness of the NES
k_e	Modal stiffness of i'th mode scaled by $e_i(\ell)^2$
k_p	Coefficient of the nonlinear NES stiffness
k_{lin}	Linear stiffness of NES
λ	Modal damping of the main system per m_{na}
λ_{na}	NES damping per m_{na}
m_e	Modal mass of i'th mode scaled by $e_i(\ell)^2$
m_{na}	Mass of NES
ω_i	The i'th eigenfrequency
Ω	Dimensionless nonlinear coefficient of NES
φ	Complexified coordinate of u
φ_{na}	Complexified coordinate of v
p	Power of NES stiffness
T_0	Fast time scale
T_1	Slow time scale
T_{pump}	The pumping time, speed of TET
T_{cascade}	The cascading time, speed of RCC
u	Coordinate of center of mass
u	Coordinate of relative NES movement
x	Displacement vector of the main system
x_ℓ	Attachment coordinate of NES
x_{na}	Coordinate of the NES
ξ	Dimensionless modal damping
ξ_{na}	Dimensionless NES damping
Z_0	Dimensionless energy in center of mass
Z_{na}	Dimensionless energy in relative NES movement
$Z_0^{\pm}$	Extrema of Z_{na} on the rve
$Z_{na}^{\pm}$	Extrema of Z_{na} on the SIM

3 System dynamics

The studied main system, a linear lumped MDOF system, is governed by the following dynamic equation:

$$M\ddot{x}(t) + C\dot{x}(t) + Kx(t) = F(t) \tag{1}$$

with $x(t) = [\, x_1(t)\ x_2(t)\ \ldots\ x_n(t)\,]^T \in \mathbb{R}^{n\times 1}$ the displacement vector, $M \in \mathbb{R}^{n\times n}$ the mass matrix, $C \in \mathbb{R}^{n\times n}$ the viscous damping matrix, $K \in \mathbb{R}^{n\times n}$ the stiffness matrix and $F \in \mathbb{R}^{n\times 1}$ the force vector. In Sect. 8, the effect of additional nonlinearity in the main system is also investigated. Assuming proportional damping ($C = aM + bK, a, b \in \mathbb{R}_+$), the n quadratic eigenvalues ω_i^2 with corresponding eigenvectors e_i are derived from:

$$\begin{aligned} &det(K - M\omega^2) = 0 \\ &(K - M\omega_i^2)e_i = 0 \end{aligned} \tag{2}$$

Let $E = [e_1 \quad e_2 \quad \ldots \quad e_n] \quad \in \mathbb{R}^{n\times n}$ be the eigenvector matrix up to a scaling, then physical coordinates can be transformed into the modal coordinates $q \in \mathbb{R}^n$ by $x(t) = Eq(t)$:

$$M_q\ddot{q}(t) + C_q\dot{q}(t) + K_q q(t) = E^T F(t) \tag{3}$$

with $M_q = E^T ME$ the diagonal modal mass matrix, $C_q = E^T CE$ the diagonal modal damping matrix and $K_q = E^T KE$ the diagonal modal stiffness matrix. The main system is effectively transformed in n decoupled linear oscillators with natural frequencies ω_i.

A NES with a connecting stiffness, consisting of a linear part and a nonlinear part of uneven positive power p, $p = 2y + 1$ with $y \in \mathbb{N}_{>0}$, is attached on the main system on physical coordinate ℓ. The compound system, depicted in Fig. 1, is described by:

$$\begin{aligned} &M\ddot{x} + C\dot{x} + Kx + m_{na}\delta_{\ell n}\ddot{x}_{na} = F \\ &m_{na}\ddot{x}_{na} + c_{na}(\dot{x}_{na} - \dot{x}_\ell) \\ &\quad + k_{\text{lin}}(x_{na} - x_\ell) + k_p(x_{na} - x_\ell)^p = 0 \end{aligned} \tag{4}$$

with $\delta_{\ell n} = [\, 0\,0\,\ldots\,0\,1\,0\,\ldots 0\,]^T \in \mathbb{R}^{n\times 1}$, the connectivity vector, nonzero at the ℓth index. The modal decomposition of the original system is substituted in the compound system:

$$\begin{aligned} &M_q\ddot{q} + C_q\dot{q} + K_q q + m_{na}e_*(\ell)^T\ddot{x}_{na} = E^T F \\ &m_{na}\ddot{x}_{na} + c_{na}(\dot{x}_{na} - \dot{x}_\ell) \\ &\quad + k_{\text{lin}}(x_{na} - x_\ell) + k_{na}(x_{na} - x_\ell)^p = 0 \end{aligned} \tag{5}$$

with $e_*(\ell) \in \mathbb{R}^{n\times 1}$ denoting the ℓth row of E, so the ℓth component of each eigenvector.

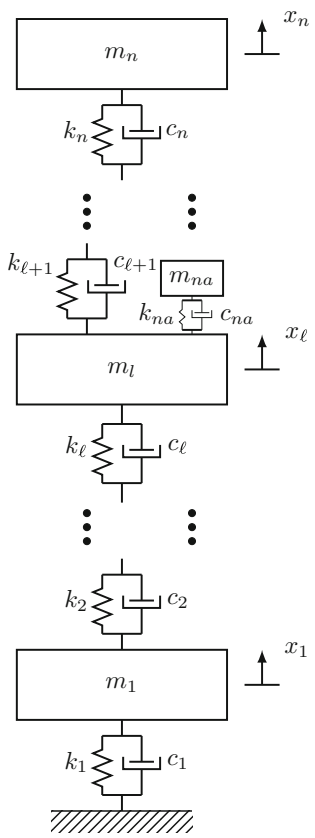

Fig. 1 The studied compound system, an MDOF linear system, with a NES attached to coordinate ℓ

In this work, the transient behavior is studied, so no force is applied, $F = 0$. Also, the system is assumed to only vibrate according to mode i:

$$x(t) = \sum_{k=1}^{n} e_k q_k(t) = e_i q_i(t) \tag{6}$$

as $q_k \neq 0$ if $k = i$. The NES is assumed to vibrate with the same frequency. This synchronous vibration is called 1:1 vibration and holds if the NES is excited near its energy threshold, [1,4]. With the single-mode assumption, internal resonances are ruled out, as then both the NES and main system vibrate with a different frequency. By replacing (6) in (4), the modal dynamics significantly simplify to:

$$\begin{aligned} &m_{q,i}\ddot{q}_i + c_{q,i}\dot{q}_i + k_{q,i}q_i + m_{na}e_i(\ell)\ddot{x}_{na} = 0 \\ &m_{na}\ddot{x}_{na} + c_{na}(\dot{x}_{na} - \dot{x}_\ell) \\ &\quad + k_{\text{lin}}(x_{na} - x_\ell) + k_p(x_{na} - x_\ell)^p = 0 \end{aligned} \tag{7}$$

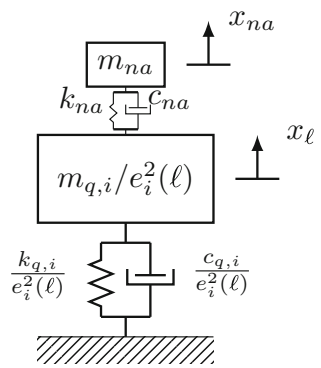

Fig. 2 Single-mode assumption of compounds system results in a 2DOF problem

This can be rewritten to only include the attachment point displacement $x_\ell = e_i(\ell)q_i$ and the NES displacement x_{na}:

$$\begin{aligned} &m_e\ddot{x}_\ell + c_e\dot{x}_\ell + k_e x_\ell + m_{na}\ddot{x}_{na} = 0 \\ &m_{na}\ddot{x}_{na} + c_{na}(\dot{x}_{na} - \dot{x}_\ell) \\ &\quad + k_{\text{lin}}(x_{na} - x_\ell) + k_p(x_{na} - x_\ell)^p = 0 \end{aligned} \tag{8}$$

By assuming a single mode of vibration, the $n+1$ DOF compound system is thus rewritten as a 2DOF problem. It is as if the NES is attached to an SDOF main system with mass $m_e = \frac{m_{q,i}}{e_i(\ell)^2}$ that is grounded with damping $c_e = \frac{c_{q,i}}{e_i(\ell)^2}$ and stiffness $k_e = \frac{k_{q,i}}{e_i(\ell)^2}$, see Fig. 2. The coordinate of the equivalent SDOF main system equals the coordinate of the attachment point of the NES on the original MDOF main system, ℓ.

Dividing (8) by m_e:

$$\begin{aligned} &\ddot{x}_\ell + \varepsilon\lambda\dot{x}_\ell + \omega_i^2 x_\ell + \varepsilon\ddot{x}_{na} = 0 \\ &\varepsilon\ddot{x}_{na} + \varepsilon\lambda_{na}(\dot{x}_{na} - \dot{x}_\ell) + \varepsilon\alpha_p(x_{na} - x_\ell)^p \\ &\quad + \varepsilon\kappa\omega_i^2(x_{na} - x_\ell) = 0 \end{aligned} \tag{9}$$

with

$$\varepsilon\lambda = \frac{c_e}{m_e} \quad \omega_i^2 = \frac{k_e}{m_e} \quad \varepsilon = \frac{m_{na}}{m_e} \quad \kappa = \frac{k_{\text{lin}}}{m_{na}\omega_i^2}$$

$$\lambda_{na} = \frac{c_{na}}{m_{na}} \quad \alpha_p = \frac{k_p}{m_{na}}$$

with $\varepsilon \ll 1$, the mass ratio, assumed to be small and κ, the dimensionless measure for the linear part of the NES.

Previous research [9–11] showed the existence of a certain initial energy threshold for $k_{\text{lin}} = 0$ and $p = 3$, below which the NES performs suboptimal, and above which TET is initiated and the energy is suddenly transferred from the main system to the NES. Under specific initial conditions, internal resonances can occur. This is not considered as it is impractical to expect specific initial conditions in a vibration mechanical system. Also, TET through internal resonance is considered sup-optimal and if they do occur, they disappear quickly when damping is present [1]. In the next section, the nonlinear dynamics of (9) are made more manageable using semi-analytic techniques.

4 Slow flow dynamics

In this section, the slow flow dynamics are derived, from which we are able to tune the NES and to define several *algebraic* performance measures for targeted energy transfer.

New variables are introduced, $u = x_l + \varepsilon x_{na}$, the center of mass of modal/absorber system (8), and $v = x_l - x_{na}$, the relative absorber movement.

In the new coordinates, (9) becomes (while omitting terms $\mathcal{O}(\varepsilon^2)$ and with $\varepsilon\ddot{u} = -\varepsilon\omega_i^2 u + \mathcal{O}(\varepsilon^2)$)

$$\begin{aligned} &\ddot{u} + \omega_i^2 u + \varepsilon\Big(\lambda\dot{u} + \omega_i^2(v - u)\Big) + \mathcal{O}(\varepsilon^2) = 0 \\ &\varepsilon(\ddot{v} + \omega_i^2 v) + \varepsilon\omega_i^2(u - v) + \varepsilon\lambda_{na}\dot{v} + \varepsilon\alpha_p v^p \\ &\quad + \varepsilon\kappa\omega_i^2 v + \mathcal{O}(\varepsilon^2) = 0 \end{aligned} \tag{10}$$

Variables u and v are assumed to vibrate with a single mode, 1:1 resonance, so they can be complexified to:

$$\begin{aligned} &\varphi(t)e^{i\omega_i t} = \dot{u} + i\omega_i u, \varphi \in \mathbb{C} \\ &\varphi_{na}(t)e^{i\omega_i t} = \dot{v} + i\omega_i v, \varphi_{na} \in \mathbb{C} \end{aligned} \tag{11}$$

with both $\varphi(t)$ and $\varphi_{na}(t)$ representing an amplitude and phase modulating function and $e^{i\omega_i t}$ an oscillation with frequency ω_i. This allows for a change of variables:

$$\begin{aligned} u &= \frac{\varphi e^{i\omega_i t} - \bar{\varphi}e^{-i\omega_i t}}{2i\omega_i} & v &= \frac{\varphi_{na}e^{i\omega_i t} - \bar{\varphi}_{na}e^{-i\omega_i t}}{2i\omega_i} \\ \dot{u} &= \frac{\varphi e^{i\omega_i t} + \bar{\varphi}e^{-i\omega_i t}}{2} & \dot{v} &= \frac{\varphi_{na}e^{i\omega_i t} + \bar{\varphi}_{na}e^{-i\omega_i t}}{2} \\ \ddot{u} + \omega_i^2 u &= \dot{\varphi}e^{i\omega_i t} & \ddot{v} + \omega_i^2 v &= \dot{\varphi}_{na}e^{i\omega_i t} \end{aligned} \tag{12}$$

4.1 Semi-analytic reduction

The complexified variables are expanded in a perturbation series:

$$\begin{aligned} \varphi &= \varphi_0 + \varepsilon\varphi_1 + \cancel{\varepsilon^2\varphi_2} + \cdots \\ \varphi_{na} &= \varphi_{na0} + \varepsilon\varphi_{na1} + \cancel{\varepsilon^2\varphi_{na2}} + \cdots \end{aligned} \tag{13}$$

which expands the variable φ (φ_{na}) into a sum of decreasingly contributing terms $\varepsilon^i\varphi_i$ ($\varepsilon^i\varphi_{nai}$). Here, both series are truncated for $\mathcal{O}(\varepsilon^2)$ and higher. This way, both φ and φ_{na} only consist of a major ($\mathcal{O}(\varepsilon^0)$), denoted by index 0 and a minor ($\mathcal{O}(\varepsilon^1)$) contribution, denoted by index 1. This technique can transform difficult-to-solve dynamics into an easily solvable problem for the ($\mathcal{O}(\varepsilon^0)$)th order term, from which the small perturbing term can be determined.

Often, the perturbation series will initially approximate the dynamics, but fail on a longer time scale. To tackle this, an additional technique is applied to the perturbation series, the multiple scales technique. The technique assumes the dynamics behave on two time scales, a fast $T_0 = t$ and a slow $T_1 = \varepsilon t$ time scale. T_0 and T_1 are assumed to be independent of each other, making the derivative w.r.t. t, up to $\mathcal{O}(\varepsilon)$:

$$\frac{\mathrm{d}}{\mathrm{d}t} = \frac{\partial}{\partial T_0} + \varepsilon\frac{\partial}{\partial T_1} \tag{14}$$

By applying multiple scales on the perturbation series, the dynamics will be approximated both initially and on the long term. For an introduction on both techniques and their combined use, please refer to [17].

Changing the variables u and v to φ and φ_{na} with (12) and applying both perturbation series and multiple time scales on (10) while omitting terms beyond $\mathcal{O}(\varepsilon^2)$ yields:

$$\begin{aligned}
&\frac{\partial\varphi_0}{\partial T_0} + \varepsilon\frac{\partial\varphi_0}{\partial T_1} + \varepsilon\frac{\partial\varphi_1}{\partial T_0} + \varepsilon\lambda\frac{\varphi_0}{2} + \varepsilon\frac{\omega_i^2}{2i\omega_i}\left(\varphi_{na0} - \varphi_0\right)\\
&\quad + \left(\varepsilon\lambda\frac{\bar{\varphi}_0}{2} - \varepsilon\frac{\omega_i^2}{2i\omega_i}\left(\bar{\varphi}_{na0} - \bar{\varphi}_0\right)\right)e^{-2i\omega_i t} = 0\\
&\varepsilon\left(\frac{\partial\varphi_{na0}}{\partial T_0}\right) + \varepsilon\frac{\omega_i^2}{2i\omega_i}\left(\varphi_0 - \varphi_{na0}\right) + \varepsilon\lambda_{na}\frac{\varphi_{na0}}{2}\\
&\quad + \frac{\varepsilon\kappa\omega_i^2}{2i\omega_i}\varphi_{na0} + \Big(-\varepsilon\frac{\omega_i^2}{2i\omega_i}\left(\bar{\varphi}_0 - \bar{\varphi}_{na0}\right)\\
&\quad + \varepsilon\lambda_{na}\frac{\bar{\varphi}_{na0}}{2} - \frac{\varepsilon\kappa\omega_i^2}{2i\omega_i}\bar{\varphi}_{na0}\Big)e^{-2i\omega_i t}\\
&\quad + \frac{\varepsilon\alpha_p}{\left(2i\omega_i\right)^p}\sum_{k=0}^{p}(-1)^k\binom{p}{k}\varphi_{na}^{p-k}\bar{\varphi}_{na}^{k}e^{i(p-2k-1)\omega_i t} = 0
\end{aligned} \tag{15}$$

The terms with a complex exponential (15) are *secular*, meaning that these terms may result in a unbounded solution. In perturbation theory, these terms are omitted. An additional motivation for this omission is that φ and φ_{na} vibrate with a single frequency, (11), while the complex exponentials would introduce extra harmonics. With the assumption of uneven power p, this results in:

$$\begin{aligned}
&\frac{\partial\varphi_0}{\partial T_0} + \varepsilon\frac{\partial\varphi_0}{\partial T_1} + \varepsilon\frac{\partial\varphi_1}{\partial T_0} + \varepsilon\lambda\frac{\varphi_0}{2}\\
&\quad + \varepsilon\frac{\omega_i^2}{2i\omega_i}\left(\varphi_{na0} - \varphi_0\right) = 0\\
&\varepsilon\left(\frac{\partial\varphi_{na0}}{\partial T_0}\right) + \varepsilon\frac{\omega_i^2}{2i\omega_i}\left(\varphi_0 - \varphi_{na0}\right)\\
&\quad + \varepsilon\lambda_{na}\frac{\varphi_{na0}}{2} + \frac{\varepsilon\kappa\omega_i^2}{2i\omega_i}\varphi_{na0}\\
&\quad - \varepsilon\frac{i\alpha_p}{\left(2\omega_i\right)^p}\binom{p}{\frac{p-1}{2}}|\varphi_{na0}|^{p-1}\varphi_{na0} = 0
\end{aligned} \tag{16}$$

The same result would be obtained if the averaging technique is performed [1]. Collecting according to powers of ε produces:

$$\begin{aligned}
&\frac{\partial\varphi_0}{\partial T_0} = 0 \quad\Rightarrow\quad \varphi_0(T_1)\\
&\frac{\partial\varphi_0}{\partial T_1} + \frac{\partial\varphi_1}{\partial T_0} + \frac{\lambda\varphi_0}{2} + \frac{\omega_i^2\varphi_{na0}}{2i\omega_i} - \frac{\omega_i^2\varphi_0}{2i\omega_i} = 0\\
&\frac{\partial\varphi_{na0}}{\partial T_0} + \frac{\lambda_{na}\varphi_{na0}}{2} + \frac{\omega_i^2\varphi_0}{2i\omega_i} - \frac{\omega_i^2(1-\kappa)\varphi_{na0}}{2i\omega_i}\\
&\quad - i\frac{\alpha_p}{(2\omega_i)^p}\left(\binom{p}{\frac{p-1}{2}}|\varphi_{na0}|^{p-1}\varphi_{na0}\right) = 0
\end{aligned} \tag{17}$$

In the first equation, it is seen that φ_0, the major contribution to φ, only varies over the slow time scale T_1. The other two equations are still difficult to solve. They feature both the derivatives in T_0 and T_1 and are coupled in φ_0, φ_1 and φ_{na0}.

It is proven in [18] that both φ_{na0} and φ_1 evolve toward a steady state as $T_0 \to \infty$; $\lim_{T_0\to\infty}\varphi_{na0} = \Phi_{na0}$ and $\lim_{T_0\to\infty}\varphi_1 = \Phi_1$, so that the dynamics of (17) can be written in steady state form of T_0, solely changing on the slow time scale T_1:

$$\begin{aligned}
&\frac{\partial\varphi_0}{\omega_i\partial T_1} = -\frac{\xi\varphi_0}{2} + \frac{i\Phi_{na0}}{2} - \frac{i\varphi_0}{2}\\
&0 = -\frac{i(1-\kappa)+\xi_{na}}{2}\Phi_{na0} + \frac{i\varphi_0}{2}\\
&\quad + \binom{p}{\frac{p-1}{2}}\frac{i\Omega}{2^p}(|\Phi_{na0}|^{p-1}\Phi_{na0})
\end{aligned} \tag{18}$$

with $\Omega = \frac{\alpha_p}{\omega_i^{p+1}}$, $\xi = \frac{\lambda}{\omega_i}$ and $\xi_{na} = \frac{\lambda_{na}}{\omega_i}$. In what follows, only the dynamics of the major contributions of the perturbation series (13) (φ_0 and φ_{na}) are analyzed and are assumed to be representative of the actual dynamics. This last claim will be verified with numerical simulations further on. The complex variables are written in polar notation; $\varphi_0(T_1) = R_0(T_1)e^{i\delta_0(T_1)}$ and $\Phi_{na0}(T_1) = R_{na}(T_1)e^{i\delta_{na}(T_1)}$ with R_0, R_{na}, δ_0 and δ_{na}

$\in \mathbb{R}$. Then splitting (18) in real and imaginary parts yields after some calculations:

$$\begin{aligned}
\frac{\partial R_0}{\omega_i \partial T_1} &= -\frac{\xi R_0}{2} - \frac{\sin(\delta_{na} - \delta_0)}{2} R_{na} \\
\frac{R_0}{\omega_i}\frac{\partial \delta_0}{\partial T_1} &= -\frac{R_0}{2} + \frac{\cos(\delta_{na} - \delta_0)}{2} R_{na} \\
0 &= -\frac{\sin(\delta_0 - \delta_{na})}{2} R_0 - \frac{\xi_{na}}{2} R_{na} \\
0 &= \frac{\cos(\delta_0 - \delta_{na})}{2} R_0 - \frac{1-\kappa}{2} R_{na} \\
&\quad + \binom{p}{p-1} \frac{\Omega}{2^p} R_{na}^p
\end{aligned} \tag{19}$$

The first and third equations are combined, as well as the third and fourth:

$$\begin{aligned}
\frac{\partial R_0^2}{\partial T_1} &= -\xi R_0^2 - \xi_{na} R_{na}^2 \\
R_0^2 &= \left[\xi_{na}^2 + \left(1 - \kappa - \frac{\binom{p}{\frac{p-1}{2}}}{2^{p-1}} \Omega R_{na}^{\frac{p-1}{2}} \right)^2 \right] R_{na}^2
\end{aligned} \tag{20}$$

The energy-like variables $E_0 = R_0^2$ and $E_{na} = R_{na}^2$ and their dimensionless counterpart, $Z_0 = \Omega^{\frac{2}{p-1}} E_0$ and $Z_{na} = \Omega^{\frac{2}{p-1}} E_{na}$, are introduced:

$$\begin{aligned}
\frac{\partial Z_0}{\partial T_1} &= -\lambda Z_0 - \lambda_{na} Z_{na} \\
Z_0 &= \left[\xi_{na}^2 + \left(1 - \kappa - \frac{\binom{p}{\frac{p-1}{2}}}{2^{p-1}} Z_{na}^{\frac{p-1}{2}} \right)^2 \right] Z_{na}
\end{aligned} \tag{21}$$

with E_0, E_{na}, Z_0 and $Z_{na} \in \mathbb{R}_+$ according to their definition. (21) describes how the (dimensionless) energy of the major contributions of φ and φ_{na} changes over the slow time T_1. It consists of the dynamics of Z_0 and a static relation, a *slow invariant manifold* (SIM), restricting Z_0 and Z_{na} on the phase plane for the slow time. The dynamics of Z_0 state that Z_0 always decreases over the slow flow time, if there is damping λ or λ_{na}. The SIM has the same shape for the class of systems with equal ξ_{na}, κ and p and is plotted for several p's and κ's as shown in Figs. 3 and 4. Previously, the importance of the SIM has been shown in [9,10], where it was shown that for $p = 3$ and $\kappa = 0$ and sufficiently low ξ_{na}, there exist a zone of Z_0 corresponding to three solutions of Z_{na} on the SIM. The existence of this zone is associated with the existence of TET. Figure 4 suggests that this zone exists for any p and κ, which is proven in the next section. The point where the solutions in Z_{na} bifurcate are used to tune the nonlinear absorber.

The relationships in (21) are of paramount importance. Not only does it give the conditions for TET, it allows to tune a NES and to define algebraic per-

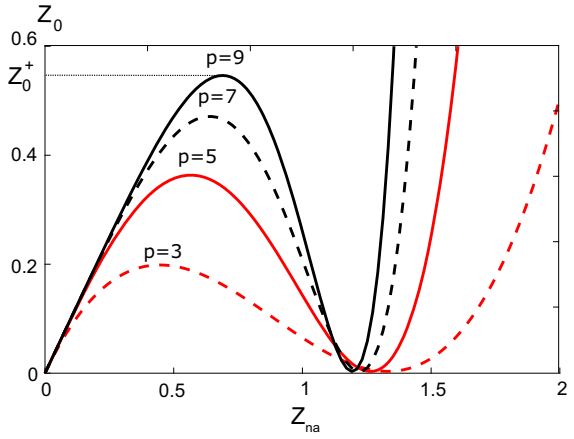

Fig. 3 The SIM, (21), for different powers, 3 (red dash), 5 (red), 7 (black dash) and 9 (black) for $\xi_{na} = 0.1$. The maximum of the SIM, Z_0^+ is denoted for $p = 9$. (Color figure online)

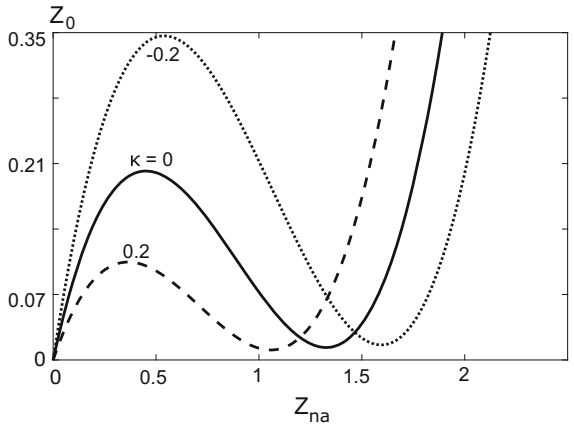

Fig. 4 The SIM, relating Z_0 and Z_{na}, for $p = 3$ and $\kappa = 0.2$ (line dash), $\kappa = 0$ (line) and $\kappa = -0.2$ (dots) for $\xi_{na} = 0.10$

formances measure of TET. As such the TET can be assessed without numerical simulation.

4.2 Slow invariant manifold analysis

It is first ascertained that the SIM, regardless of p and κ, has 3 solutions in Z_{na} in a range of values of Z_0. If this holds, the NES can be tuned by using the maximum of the SIM, as is done for the case $\kappa = 0$ & $p = 3$ [9,10]. The number of extrema of the SIM determines the solutions of Z_{na} on the SIM for a given Z_0. To find the extrema, the SIM, (21), is derived w.r.t. Z_{na}:

$$\frac{\partial Z_0}{\partial Z_{na}} = \frac{p\binom{p}{\frac{p-1}{2}}^2}{2^{2(p-1)}} Z_{na}^{p-1} - (1-\kappa)\frac{(p+1)\binom{p}{\frac{p-1}{2}}}{2^{p-1}} Z_{na}^{\frac{p-1}{2}} + (1-\kappa)^2 + \xi_{na}^2 \tag{22}$$

For $p = 3$ and $\kappa = 0$ it was already shown that there is one maximum followed by one minimum, asserting an interval of Z_0 having three solutions of Z_{na}. For any power p (22) is a quadratic equation in $Z_{na}^{\frac{p-1}{2}}$. For $Z_{na}^{\frac{p-1}{2}}$ to have two real solutions, the discriminant has to be positive; so if $(1-\kappa)^2(p+1)^2 - 4p((1-\kappa)^2+\xi_{na}^2) > 0$ or

$$\xi_{na} < \frac{(p-1)(1-\kappa)}{2\sqrt{p}} \tag{23}$$

which also implies that $\kappa < 1$ as the dimensionless damping $\xi_{na} \in \mathbb{R}_+$. This condition has to be met to ensure extrema and therefore to ensure TET. It is remarkable that while $\kappa = 1$ ensures a performant linear absorber, it completely diminishes the performance of a NES, as there is no TET.

As both Z_{na} and $Z_0 \in \mathbb{R}_+$ according to their definition, the two solutions of $Z_{na,1,2}^{\frac{p-1}{2}}$ should be $\in \mathbb{R}_+$ as only then the $\frac{p-1}{2}$-root of the solution, $Z_{na,1,2}, \in \mathbb{R}_+$. The sum and product of the solutions of a quadratic equation are related to the coefficients of (22):

$$\begin{aligned} Z_{na,1}^{\frac{p-1}{2}} + Z_{na,2}^{\frac{p-1}{2}} &= \frac{2^{2(p-1)}(1-\kappa)(p+1)}{p\binom{p}{\frac{p-1}{2}}} \\ Z_{na,1}^{\frac{p-1}{2}} Z_{na,2}^{\frac{p-1}{2}} &= 2^{2(p-1)}\frac{(1-\kappa)^2+\xi_{na}^2}{p\binom{p}{\frac{p-1}{2}}^2} \end{aligned} \tag{24}$$

As the two solutions should be positive, the left sides of both equations in (24) are positive. The right sides of both equations are both positive if $\kappa < 1$ (which itself is already a condition for TET). This confirms that there are only two real positive $Z_{na,1,2}$ for which the derivative, (22), is zero. By computing the second derivative, it can be shown that the first extrema is a maximum, and the second a minimum.

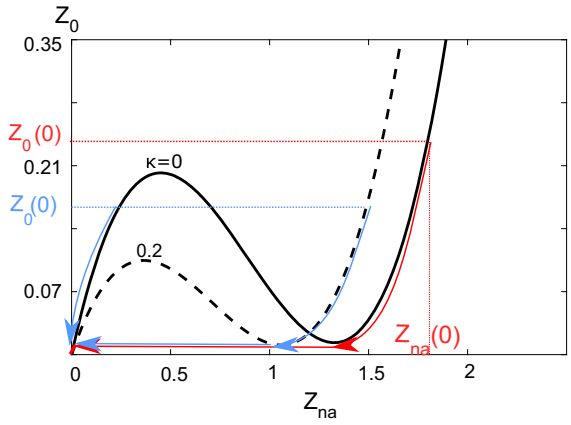

Fig. 5 Two typical descents down the SIM for $\kappa = 0$ and $\kappa = 0.2$

It can be concluded that for any uneven positive power p, the SIM has this same interval of three solutions, as long as the condition on (23) is met. The extrema of Z_{na} and Z_0 are:

$$\begin{aligned} Z_{na\pm}^{\frac{p-1}{2}} &= \frac{2^{p-2}}{p\binom{p}{\frac{p-1}{2}}}\Big((1-\kappa)(p+1) \pm \sqrt{(p-1)^2(1-\kappa)^2 - 4p\xi_{na}^2}\Big) \\ Z_0^{\pm} &= \left[\xi_{na}^2 + \left(1-\kappa-\frac{\binom{p}{\frac{p-1}{2}}}{2^{p-1}} Z_{na\mp}^{\frac{p-1}{2}}\right)^2\right] Z^{na\mp} \end{aligned} \tag{25}$$

with the $-$ index denoting the lower value solution and $+$ index the higher value of the two.

In previous research, it was shown that as long as the initial energy of the linear mode, $Z_0(0)$, is larger than the maximum Z_0^+, TET is initiated [9,10]. So besides the parameter condition (23), a threshold on the initial conditions or energy exists as well. If TET is initiated, the slow time dynamics will behave according to (21); not only will Z_0 decrease, Z_0 and Z_{na} behave according to the SIM. TET continues as long as $Z_0 > Z_0^-$, after which another bifurcation occurs on the SIM and Z_0 will decrease slowly. Figure 5 shows a typical descent down the SIM, when TET is initiated drawn in red, and when TET is not initiated, drawn in blue (the blue on

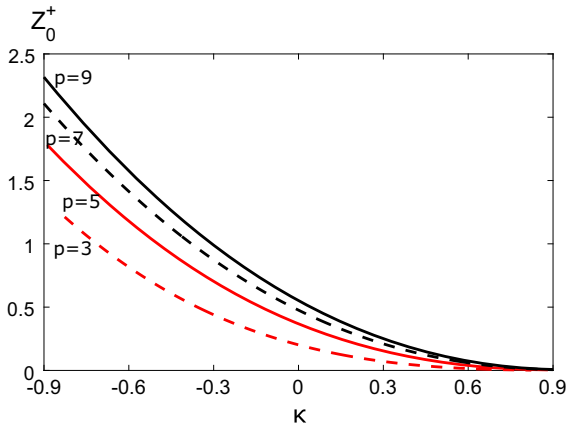

Fig. 6 The threshold of the dimensionless energy for several powers p 3 (red dash), 5 (red), 7 (black dash) and 9 (black), in function of κ for $\xi_{na} = 0.1$. (Color figure online)

the $\kappa = 0$ curve). For the case when $Z_0 < Z_0^-$, the curve will initiate on the left-most solution, [9,10].

4.3 Tuning absorber

With complete knowledge of the SIM and its extrema, the NES can be tuned. As long as the initial linear mode energy, $Z_0(0) = \Omega^{\frac{2}{p-1}}|\varphi_0(0)|^2 \geq Z_0^+$ or, in terms of the dimensionless nonlinear NES coefficient:

$$\Omega^{\frac{2}{p-1}} \geq \frac{Z_0^+}{|\varphi_0(0)|^2} \tag{26}$$

TET is initiated. If Ω is chosen too high, $Z_0(0) \gg Z_0^+$, the targeted energy transfer will be a lot slower. It was shown in [1,9,10] that if $Z_0(0) = Z_0^+$, the most optimal TET occurs. It is important to have full knowledge of the initial conditions $\varphi_0(0)$ to design the most optimal absorber.

To calculate the initial conditions of $\varphi_0(0)$, the minor contribution in (13) is neglected, so $\varphi_0(0) \approxeq \varphi(0) = \dot{u}(0) + i\omega_i u(0)$. Consequently the absorber nonlinearity can be calculated according to (26):

$$k_p \geq \frac{m_{na}\omega_i^{p+1}(Z_0^+)^{\frac{p-1}{2}}}{\left(\dot{u}^2(0) + \omega_i^2 u^2(0)\right)^{\frac{p-1}{2}}} \tag{27}$$

The influence of κ and p on Z_0^+ is shown in Fig. 6. For increasing κ, the threshold value Z_0^+ decreases. This has several consequences. First, the optimal nonlinear coefficient k_p decreases as κ increases, if the absorber is tuned with the same initial conditions $u(0)$ and $\dot{u}(0)$. Second, κ is capable of handling changing operating conditions. When (27) has been applied for the case $\kappa = 0$, a decrease in initial condition can make that $Z_0(0) < Z_0^+$ meaning no TET is engaged and energy dissipation is slow. By retrofitting a carefully designed $\kappa > 0$, the position of Z_0^+ can be adjusted to again ensure TET. Figure 5 shows two SIM, respectively, $\kappa = 0$ (black) and $\kappa = 0.2$ (black dash) with two different initial conditions in red and blue. While the red descent is initially still above the threshold for $\kappa = 0$, this is not the case if the initial conditions decrease, the blue descent. By introducing a linear part, $\kappa = 0.2$, the threshold value Z_0^+ is lowered so that TET is engaged once again.

5 Targeted energy transfer performance measures

Few attempts have been made to quantify performance of TET, with the goal of improving the NES performance. Often, for a numerical example, the total amount of dissipated energy during TET is investigated through simulation, while the speed of TET is not considered [1,3–6,14]. In these studies, the coefficient of the NES nonlinearity is not varied to asses the change in TET performance.

By introducing a linear stiffness in the NES, κ, and different powers of p, the influence of these parameters on TET performance should be investigated, not only on the total amount of energy dissipated on the NES, but also how the speed of TET changes. From here on, some performance measures are defined from the SIM (21), with only 3 parameters to consider, ξ_{na}, p, and κ. Not only are the parameters to be considered reduced, the expressions derived are algebraic equations, requiring no simulations, allowing us to quickly assess influence of any parameter on TET performance.

In [10], Nyugen defined an *energy dissipation* and *pumping time*, both derived from an SIM, similar as in this research. The energy dissipation is the fraction of the energy dissipated during TET, which is similar in meaning as the previously considered performance measure in the literature. The major difference is that Nyugen's energy dissipation does not require a numerical simulations and is algebraic, depending only the main system and NES's parameters. The pumping time is a measure of TET speed. It was shown that the TET is the fastest when the NES is tuned such that $Z(0)_0 = Z_0^+$. Both measures were only determined for

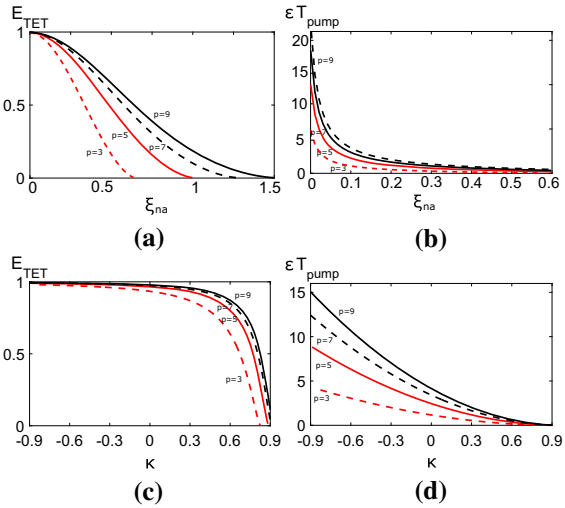

Fig. 7 The energy dissipation during TET, E_{TET} (**a**, **c**) and pumping time T_{pump} (**b**, **d**); for several powers p; 3 (red dash), 5 (red), 7 (black dash) and 9 (black), (**a**, **b**) in function ξ_{na} and $\kappa = 0$ and (**c**, **d**) in function of κ for $\xi_{na} = 0.1$ (**c**, **d**). Each time $Z_0(0) = Z_0^+$ to ensure the most optimal TET. (Color figure online)

a cubic nonlinearity and studied under variations in the damping ξ_{na}. Just as the energy dissipation, the major advantage of the pumping time is its algebraic nature.

Below, the dissipated energy and pumping time definitions of Nyugen are extended for general positive uneven powers p and an additional (positive or negative) linear stiffness κ, while also introducing the amplitude reduction and average TET power as new performance measures.

5.1 Energy dissipation & amplitude reduction

The energy dissipation during TET is defined as:

$$E_{\text{TET}} = 1 - \frac{Z_0^-}{Z_0(0)} = 1 - \frac{E_0^-}{E_0(0)} \tag{28}$$

It is a measure for the dissipation of the initial energy in the linear mode ($Z_0(0)$) during TET. The remaining energy Z_0^- is absorbed very slowly.

A similar quantity can be defined for the reduction in vibration amplitude during TET, rather than the energy:

$$A_{\text{TET}} = 1 - \sqrt{\frac{E_0^-}{E_0(0)}} = 1 - \frac{R_0^-}{R_0(0)} \tag{29}$$

with $R_0^- = \sqrt{E_0^-}$.

These measures are only relevant if TET will occur, so if $E_0(0) > E_0^+$. Figure 7a shows E_{TET} in function of ξ_{na} and p. The amount of energy dissipated during TET decreases as the damping increases. This will be the limiting factor in the choice of ξ_{na}. E_{TET} is also plotted in function of κ and p as shown in Fig. 7c. It is observed that if p increased or κ decreases, more of the initial energy is dissipated during TET.

5.2 The pumping time

Consider the slow-time change of the energy stored in the relative absorber displacement, derived from (21):

$$\frac{1}{\omega_i}\frac{\partial Z_{na}}{\partial T_1} = \frac{-\xi_{na} Z_{na} - \xi Z_0}{\frac{p\left(\frac{p}{\frac{p-1}{2}}\right)^2}{2^{2(p-1)}} Z_{na}^{p-1} - (1-\kappa)\frac{(p+1)\left(\frac{p}{\frac{p-1}{2}}\right)}{2^{p-1}} Z_{na}^{\frac{p-1}{2}} + (1-\kappa)^2 + \xi_{na}^2} \tag{30}$$

When neglecting the main system's When neglecting the main system's modal damping ξ, separation of the variables Z_{na} and T_1 is possible. When subsequently integrated, this yields:

$$\begin{aligned} I(Z_{na}) = {} & \frac{p\left(\frac{p}{\frac{p-1}{2}}\right)^2}{(p-1)2^{2(p-1)}} Z_{na}^{p-1} \\ & - \frac{\left(\frac{p}{\frac{p-1}{2}}\right)(1-\kappa)(p+1)}{\frac{p-1}{2}2^{p-1}} Z_{na}^{\frac{p-1}{2}} \\ & + \left((1-\kappa)^2 + \xi_{na}^2\right) ln(Z_{na}) = C - \omega_i \xi_{na} T_1 \end{aligned} \tag{31}$$

with C the integration constant. In Sect. 8, the effect of modal damping is investigated, which does not allow separation of variables. It is not derived here as some observations of the simulations need to be made first.

The expression (31) can be used to determine the time between two energy states $Z_{na,1}$ and $Z_{na,2}$:

$$\varepsilon T_{1\to 2} = \frac{1}{2\pi\xi_{na}}\Big(I(Z_{na,1}) - I(Z_{na,2})\Big) \tag{32}$$

with $T_{1\to 2}$ the time relative to the linear mode's natural period $\big(T_1(Z_{na,1}) - T_1(Z_{na,2})\big) \cdot \frac{\omega_i}{2\pi}$. On the SIM, $Z_0(0)$ has a corresponding $Z_{na}(0)$ (Fig. 5). If the initial energy $Z_{na}(0)$ exceeds the energy threshold (so $Z_0(0) > Z_0^+$), TET will persist from $Z_{na}(0)$ until the minimum of the SIM, Z_{na}^+, allowing us to define the pumping time T_{pump} as:

$$\varepsilon T_{\text{pump}} = \frac{1}{2\pi\zeta_{na}}\Big(I(Z_{na}(0)) - I(Z_{na}^+)\Big) \tag{33}$$

Both the pumping time T_{pump} and energy dissipation E_{TET} are algebraic expressions and are determined without any numerical simulation, which allows us to quickly asses the influence of parameter changes on the performance of TET. This is a huge advantage over previous TET performances measures, which require simulations to be assessed. In Fig. 7b, the optimal ($Z_0(0) = Z_0^+$) pumping time is shown in function of ξ_{na} and p for $\kappa = 0$. An increased damping will speed up the TET, however, a decreased amount of energy will be dissipated. To ensure a significant fraction of the energy is dissipated, ξ_{na} will be chosen as 0.1 in the numerical examples.

In Fig. 7d, the optimal ($Z_0(0) = Z_0^+$) pumping time is shown in function of κ and p. The pumping time increases as $p > 3$ and $\kappa < 0$ and decreases as $\kappa > 0$ increases. By observing both figures in Fig. 7, increasing κ to decrease T_{pump} comes at a cost, as E_{TET} decreases as well.

With regard to TET speed, in [6], an opposite conclusion was stated for $p > 3$. It is claimed that for increasing power p, TET is expedited, while the opposite is claimed here. The difference between this paper and [6], is that in their given numerical example, the nonlinear coefficient α_p in [6] was constant while only the power p changed. This way, the NES coefficient was not optimally tuned for each power, and seemingly an increased power sped up TET. While their NES for $p = 7$ was near optimal tuning, the same α_p for $p = 3$ and $p = 5$ leads to a highly unoptimally tuned NES.

For the class of systems with same ξ_{na}, p and κ, (33) still depends by the mass ratio ε. By inspecting (33), one would advise increasing ε to decrease T_{pump}, achieving faster TET. Yet from an application point of view, a small ε is a highly desired feature for vibration absorbers. Besides practical limitations, the whole semi-analytic analysis also relies entirely on a small ε. Therefore, just increasing the mass ratio is not suggested to optimize the NES. Also, the actual dynamics, (4), do not start on the SIM, as initially, $Z_{na}(0)$ does not depend on $Z_0(0)$. The SIM only hold on a slow time scale. In fact, simulations show a transient behavior before *attracted* to the SIM, [10]. To ensure the attraction to the SIM, T_{pump}, should be at least a few periods, or else no TET will occur. This also means ε should not be too large.

5.3 The average TET power, $\bar{P}_{\text{TET}}$

With both a measure for energy dissipation (E_{TET}) and speed (T_{pump}), an average power-like measure can be defined:

$$\bar{P}_{\text{TET}} = \frac{E_{\text{TET}}}{T_{\text{pump}}} \tag{34}$$

6 Numerical study and comparison of actual dynamics with slow flow

In the previous section, the nonlinear dynamics of (9) have been significantly simplified to a linear dynamic equation and a nonlinear static relation (21). From these simplified equations, the conditions to ensure TET were stated and NES tuning rules were established. Furthermore, several performance measures for TET were derived, most importantly the pumping time T_{pump} and the dissipated energy E_{TET}. Also, several properties of the nonlinear absorber were discussed; $\kappa > 0$ can reduce the nonlinear coefficient k_p, $\kappa > 0$ hastens the targeted energy transfer, while increasing p and $\kappa < 0$ on the other hand impede TET.

When compared to existing literature, the strength in the performance measures presented in previous section, is that they are algebraic, and do not require any numerical simulation to be determined. All of the measures and properties were derived from the so-called slow time dynamics (21). However, the question remains if these measures hold their merit for actual numerical simulations of (4). Therefore, the actual dynamics and the slow flow dynamics are simulated and compared for similarity for the SDOF main system presented in Fig. 8, with numerical values found in Table 1. The choice is made for $\xi_{na} = 0.1$ as Fig. 7a, b shows that a significant amount of the energy is dissipated in a short time.

6.1 Performance measures and tuning

For the given $\xi_{na} = 0.1$, the influence of κ and p on the TET performance was plotted as shown in Fig. 7. Increasing κ has a positive influence on the pumping time T_{pump}, however this came with a sacrifice, as the dissipated energy E_{TET} also decreases.

The NES is tuned for $\dot{x} = 0.1$ for several choices of κ and p, with coefficients k_p and k_{lin}, and measures E_{TET}

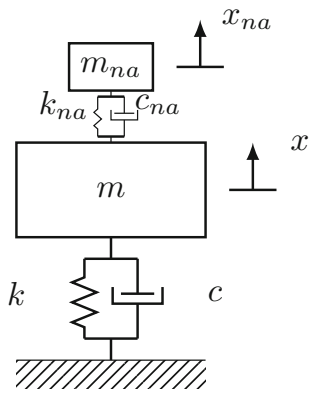

Fig. 8 An SDOF main system with a NES

Table 1 Numerical values for SDOF system, Fig. 8. The absorber damping is chosen as such that $\xi_{na} = 0.1$

Parameter	Value
m [kg]	1
k [$\frac{\text{N}}{\text{m}}$]	1
c [$\frac{\text{Ns}}{\text{m}}$]	0
m_{na} [kg]	0.02
c_{na} [$\frac{\text{Ns}}{\text{m}}$]	0.002

Table 2 The nonlinear coefficient, dissipated energy during TET, E_{TET} and pumping time T_{pump} for several p and κ

p & κ	Z_0^+	k_p	k_{lin}	E_T	$T_{\text{pump}}\frac{\omega_i}{2\pi}$
$p = 3\ \kappa = 0$	0.2020	0.444	0	0.940	63.9
$p = 3\ \kappa = 0.2$	0.1047	0.230	0.004	0.908	40.13
$p = 3\ \kappa = -0.2$	0.3467	0.763	-0.004	0.958	92.95
$p = 5\ \kappa = 0$	0.3677	29.75	0	0.967	128
$p = 7\ \kappa = 0$	0.4761	2373	0	0.975	176

and T_{pump} in Table 2. The nonlinear coefficient k_p is chosen 10% higher than its minimal value determined with (27), so $Z_0(0)$ is slightly higher than Z_0^+, to ensure the actual fast dynamics are attracted to the SIM [9,10].

6.2 Comparison of slow flow and actual dynamics

To compare an actual numerical simulation of (4) with slow flow simulation (21), equivalent energy variables are defined for the actual, fast, dynamics:

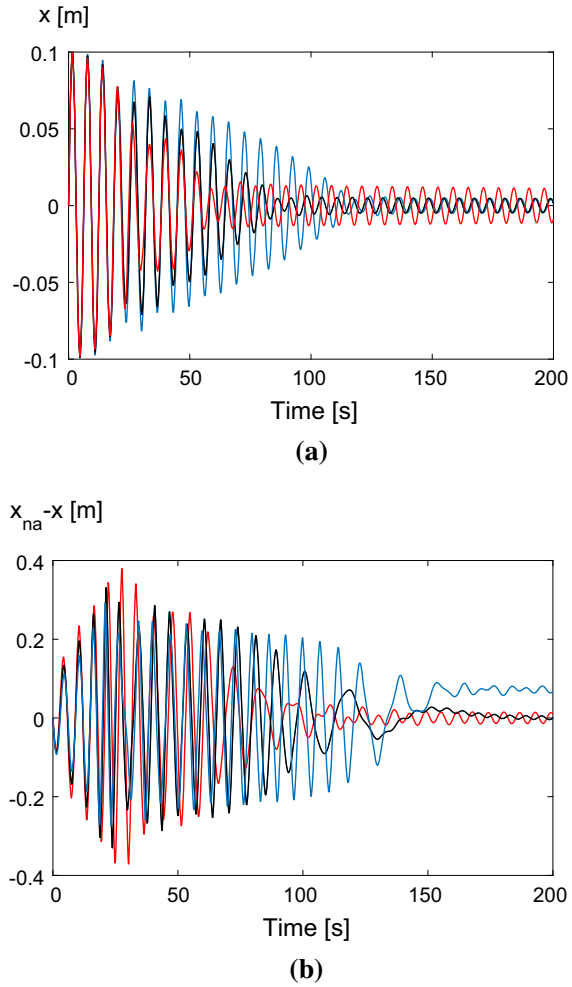

Fig. 9 Numerical simulation of system Fig. 8 for $\dot{x}(0) = 0.1$, $p = 3$ and $\xi_{na} = 0.1$. Main system vibration (**a**) and NES (**b**) for $\kappa = 0$ (black), $\kappa = 0.2$ (red) and $\kappa = -0.2$ (blue). (Color figure online)

$$E_{0,\text{fast}} = \dot{u}^2 + \omega_i^2 u^2$$
$$E_{na,\text{fast}} = \dot{v}^2 + \omega_i^2 v^2 \tag{35}$$

The dissipated energy during TET, E_{TET} and the pumping time T_{pump} are also given for each case. To confirm that these metrics actually hold, the system dynamics are simulated next.

6.3 Simulations

First, the case where $p = 3$ is compared for the different values of κ. Fig. 9a, b shows the time evolutions

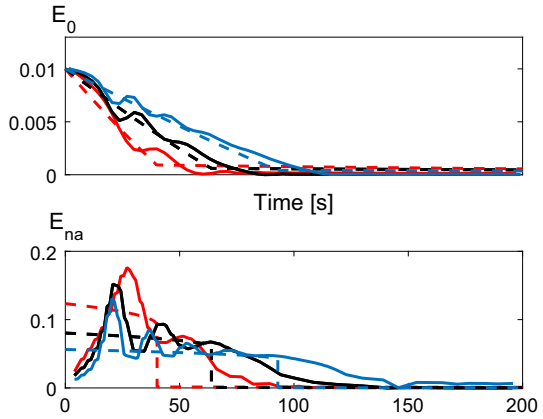

Fig. 10 Comparison of slow flow dynamics (dashed) with actual dynamics (solid) for $\kappa = 3$ (black), $\kappa = 0.1$ (red) and $\kappa = -0.1$ (blue)). (Color figure online)

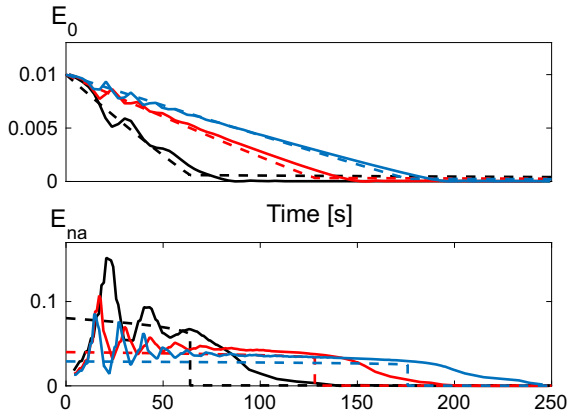

Fig. 11 Comparison of slow flow dynamics (dashed) with actual dynamics (solid) for $p = 3$ (black), $p = 5$ (red) and $p = 7$ (blue). (Color figure online)

of, respectively, the main system and the NES of the numerical simulation of the actual dynamics. Clearly the linear component of the stiffness influences the dynamics as expected; if $\kappa > 0$ TET is faster and consequently the vibrations in the main system are reduced a lot faster then when $\kappa = 0$ and $\kappa < 0$. It is remarkable that the addition of a such small linear stiffness, $k_{\text{lin}} = \pm 0.004\ \frac{\text{N}}{\text{m}}$ changes the performance to such an extent. The amount of dissipated energy during TET is predicted as well, as when $\kappa = 0$ and $\kappa < 0$ more energy is dissipated then for $\kappa > 0$.

To verify the actual value of the performance metrics, the slow flow is simulated and the evolutions of E_0 and E_{na} are overlaid by their equivalent energies from the numerical simulation of (4), (35). The result is shown in Fig. 10. The pumping time is clearly seen in the slow dynamics as either the jump in E_{na} or the sudden change of slope in E_{na}. $E_{0,\text{fast}}$ clearly follows its slow flow equivalent but $E_{na,\text{fast}}$ behaves differently. Initially, the actual dynamics need to be attracted to the SIM. This happens while the NES heavily vibrates. This attraction part is also called *nonlinear beating* [1] for its excessive vibrations. After the nonlinear beating, $E_{na,\text{fast}}$ roughly follows its slow flow equivalent. As the energy is dissipated in the NES, E_0 will descent to its minimum on the SIM, E_0^-. On the slow time scale, E_{na} then jumps, while this immediate change of value is not followed at all by the fast dynamics. Even then, the pumping time T_{pump} and dissipated energy E_{TET}, both derived metrics from the slow flow, are still valuable for the actual system. It is clearly visible in the dynamics of $E_{0,\text{fast}}$, Fig. 9a, that the significant reduction in vibration (= TET) does cede roughly around T_{pump} and the absorbed energy during TET does roughly equal the dissipated energy. These simulations show that the slow flow dynamics are representative for the actual dynamics, and that slow flow performance measures are very valuable in predicting the performance of the NES. This allows us to quantify TET performance, and to optimize nonlinear absorbers without performing many simulations, as (28) and (33) are simple algebraic expressions. To visualize the dynamics, the phase plane of Z_0 and Z_{na} is plotted as shown in Fig. 12a–c. The slow flow dynamics follow the SIM, while the actual, fast, dynamics first need to be attracted to the SIM, only follows the SIM on average, and behaves differently near the bifurcation point.

The influence of the power p on the dynamics is shown in Fig. 11. Again the actual pumping time and energy dissipation behave as predicted in Table 2; the higher the power, the slower the TET. Similar as before, the SIMs are plotted as shown in Fig. 12d, e, yet compared to Fig. 12a–c, the slower the TET is, the better the actual dynamics follow the slow time SIM.

From the numerical simulations in this section it can be said:

- As predicted from the slow flow dynamics, the TET slows down for higher power p and the negative linear part κ.
- By defining a similar energy as the slow flow E_0, E_{na}, but for the actual dynamics, (35), it is seen

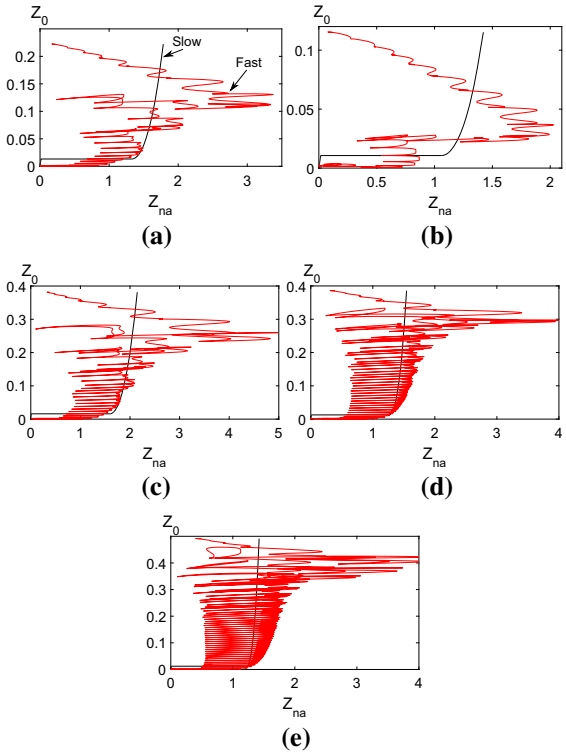

Fig. 12 Comparison of Z_{na} and Z_0 both from the slow dynamics simulation, which follows the SIM (black) and from the actual dynamics (red), calculated from (35). **a**–**c** are for $p = 3$, $\kappa = 0$, 0.2 and -0.2, respectively. **d**, **e** are for $p = 5$ and $p = 7$. (Color figure online)

that the slow flow dynamics, when simulated, are representative for the actual dynamics
- The algebraic performance measures T_{pump} and E_{TET} hold up for the actual dynamics. As a consequence, the influence of parameters on the performance of the NES can be determined without any numerical simulation.
- The relation $E_0(E_{na})$ follows the exact SIM for the slow dynamics. In the fast dynamics, first, the dynamics need some time to be attracted to the SIM. Then, the slower the TET is, the more the actual dynamics fit the SIM shape of the slow flow. This means that the performance measures are more precise for cases when TET is suboptimal.

7 Multi-modal vibrations and resonance capture cascading

The ability of a single NES to absorb multi-modal vibrations is one of its major advantages. The mechanism of multi-modal vibration absorption is called *resonance capture cascading* (RCC). It was first thoroughly investigated in the context of NES in [15]. In short the mechanism of RCC is:

- The main system is subjected to an initial condition, meaning that each mode of the main system has an initial energy. The main system starts to vibrate according to its modes
- The NES will start to vibrate with a single-mode ω_i, until a bifurcation occurs when the energy in mode i has decreased significantly. TET has actually occurred for mode i
- Next, if there is enough energy in mode $i-1$, the NES vibrates with mode ω_{i-1}, also until a bifurcation occurs,
- This *cascading* of modes continues until mode 1, after which the vibrations in the main system have been reduced for all modes.

This way, the vibrations of a multi-modal main system is absorbed by a single NES. This is in sharp contrast with linear vibration absorbers, where one absorber is able to dissipate vibrations of one mode only. Kerschen also called it multi-modal targeted energy transfer [16], as just like the single-mode TET, a certain initial energy was required to initiate strong energy transfer. Also, he showed that the initial energy level determines which mode i initiates the RCC.
Contemporary works on the subject of RCC focus on merely showing the existence of the phenomenon, while optimizing the performance or tuning a NES for specific RCC behavior has not been considered. Recently [14], a numerical study on the performance of a NES on an MDOF system was performed. However, the author of that paper only analyses a single-mode case, did not consider RCC, and performed many numerical simulations to obtain surfaces addressing the performance. Here, the objective is to analyze RCC performance algebraically, without any numerical simulations In this section, the tuning rules and performance measures derived for single-mode vibrating systems are extended to a multi-modal vibration main system. Although all the theoretical concepts of this research were developed for single-mode vibrating systems (be it SDOF or MDOF main system), it is shown that the algebraic performance measures E_{TET} and especially T_{pump} are still valid and valuable for multi-modal systems. This is because at a given time, only a single mode interacts with the NES, even though the main

system vibrates with multiple modes. First, a kind of modal decomposition of the initial condition is introduced. This artificial modal decomposition will allow to asses each mode separately, as a single-mode case, allowing us to apply the theory of Sects. 4 and 5.

7.1 Modal decomposition of initial conditions

When the NES initially vibrates with mode ω_i, the energy of the other modes is either kept in the system, or is dissipated in the main system's damping. Here the former is assumed, so $C = 0$ in (4). This way, the initial energy of each mode stays in the system until the mode is *cascaded* in the RCC.

The concepts of energy dissipation E_{TET} and pumping time T_{pump}, although developed for single-mode vibrating systems, are now expanded to the multi-modal RCC, to allow us to quantity the influence of κ and p on RCC performance. For this, the initial conditions of the physical coordinates are decomposed as initial modal conditions:

$$\dot{x}(0) = \sum_{k=1}^{n} \dot{x}^{[k]}(0) = \sum_{k=1}^{n} e_k \dot{q}_k(0) \tag{36}$$

with $\dot{x}^{[k]}(0) = e_k \dot{q}_k(0) \in \mathbb{R}^n$ the hypothetical initial speed as if only mode k is present. From here on only an initial speed is considered, but (36) can easily be expanded to include initial displacements as well. The RCC will begin at mode i, and the NES initially only vibrates with ω_i. If, hypothetically, the whole system only vibrates with mode i, the initial condition on the system would be

$$\dot{x}^{[i]}(0) = e_i \dot{q}_i(0) \tag{37}$$

This hypothetical situation allows us to apply tuning for this single-mode vibration. The hypothetical initial speed at the attachment point x_ℓ of the NES is $\dot{x}_\ell^{[i]}(0) = e_i(\ell)\dot{q}_i(0) \neq \dot{x}_\ell(0)$, which allows for tuning with (27). In this way the initial energy is associated with mode i and the NES will start to vibrate with ω_i, while the remaining modes stay contained in the main system, not interacting with the NES.

7.2 Cascading time

From the hypothetical single-mode vibration i with initial condition $\dot{x}_0^{[i]}$, both an $E_{\text{TET},i}$ and pumping time $T_{\text{pump},i}$ can be calculated. For the same NES, an $E_{\text{TET},i-1}$ and pumping time $T_{\text{pump},i-1}$ is found by assuming a single vibration with the next mode $i-1$ and its corresponding initial condition on the attachment point $\dot{x}_\ell^{[i-1]}(0) = e_{i-1}(\ell)\dot{q}_{i-1}(0)$. (The NES was tuned for mode i, it is not retuned for mode $i-1$). This proceeds from mode $i-2$ until mode 1. As RCC is a multi-modal TET, $T_{\text{pump},i}$ is interpreted as the pumping time of TET for mode i. Because the main system is undamped, the initial energy of mode $i-1$ is kept completely in the system. So after TET of mode i, TET for mode $i-1$ will occur for $T_{\text{pump},i-1}$, and so on until mode 1.

It is now postulated that this single-mode pumping time $T_{\text{pump},k}$ is actually the time of targeted energy transfer with mode k, before cascading to mode below it, $k-1$. The total cascading time then is

$$T_{\text{cascade}} = \sum_{k=1}^{i} T_{\text{pump},k} \cdot \frac{\omega_k}{2\pi} \tag{38}$$

Although there is no proof for this to hold, and the modal decomposition in quite artificial, the fact that previous research show that the NES vibrates sequentially and in descending order with the resonance frequencies of the main system motivates this hypothesis. Next, a numerical example will be presented that confirms the hypothesis.

Table 3 Numerical values for MDOF and absorber system, Fig. 13. The absorber damping is chosen as such that $\xi_{na} = 0.1$ for mode 3

Parameter	Value
m_k [kg]	1
k_k [$\frac{\text{N}}{\text{m}}$]	1
c_k [$\frac{\text{Ns}}{\text{m}}$]	0
m_{na} [kg]	0.06
c_{na} [$\frac{\text{Ns}}{\text{m}}$]	0.0108

7.3 Test of hypothesis for $p = 3$ and $\kappa = 0$

To numerically verify the cascading time hypothesis, a 3DOF main system, with numerical values in Table 3, is fitted with a NES on x_2, Fig. 13. The unity modal mass scaled eigenvector matrix of the main system and the eigenfrequencies are:

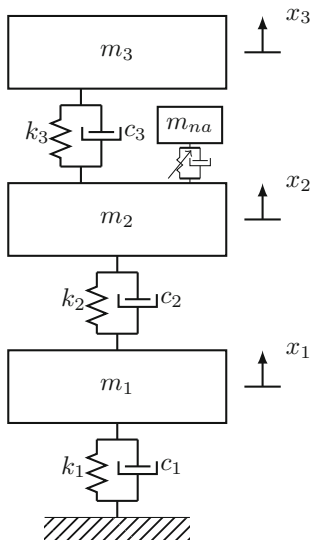

Fig. 13 A 3 degree MDOF system with a NES on floor 2 (**a**) and a NES on floor 1 and 2 (**b**), used in the numerical examples of, respectively, Sect. 7

$$E = \begin{bmatrix} 0.328 & -0.737 & 0.591 \\ 0.591 & -0.325 & -0.737 \\ 0.737 & 0.591 & 0.328 \end{bmatrix}$$
$$\omega_i = \begin{bmatrix} 0.445 \\ 1.247 \\ 1.802 \end{bmatrix} \frac{\text{rad}}{s} \tag{39}$$

The absorber mass is chosen as 2 % of the entire main system's mass. The initial condition are $\dot{x}_1(0) = 0.1\ \frac{\text{m}}{\text{s}}$ and $\dot{x}_2(0) = \dot{x}_3(0) = 0\ \frac{\text{m}}{\text{s}}$, decomposed according to (36):

$$\begin{aligned} \dot{x}(0) = e_1\dot{q}_1(0) + e_2\dot{q}_2(0) + e_3\dot{q}_3(0) \Leftrightarrow \\ \begin{bmatrix} 0.1 \\ 0 \\ 0 \end{bmatrix} = \begin{bmatrix} 0.328 \\ 0.591 \\ 0.737 \end{bmatrix} \cdot 0.0328 \\ + \begin{bmatrix} -0.737 \\ -0.328 \\ 0.591 \end{bmatrix} \cdot -0.0737 + \begin{bmatrix} 0.591 \\ -0.737 \\ 0.328 \end{bmatrix} \cdot 0.0591 \end{aligned} \tag{40}$$

Notice that on the attachment point of the NES, x_2, there is no initial condition. Now, the initial condition decomposition is used to tune the NES. The NES is tuned to mode 3, so that each mode is captured in the cascade. The hypothetical initial conditions of the single-mode vibration ω_3 is:

Table 4 The nonlinear coefficient, dissipated energy during TET, E_{TET} and pumping time T_{pump}

p & κ	Z_0^+	k_p	k_{lin}	$T_{\text{pump},3}\frac{\omega_3}{2\pi}$
$p = 3\ \kappa = 0$	0.2020	74.1	0	21.8
$p = 3\ \kappa = 0.1$	0.1480	54.3	0.0195	17.5
$p = 3\ \kappa = -0.1$	0.2678	98.2-0.0195		26.5
$p = 5\ \kappa = 0$	0.3677	29.75	0.967	43.6
$p = 7\ \kappa = 0$	0.4761	2373	0.975	59.9

Table 5 Pumping time for each mode and the cascade time

p & κ	$T_{\text{pump},3}\frac{\omega_3}{2\pi}$	$T_{\text{pump},2}\frac{\omega_2}{2\pi}$	$T_{\text{pump},1}\frac{\omega_1}{2\pi}$	T_{cascade}
$p = 3\ \kappa = 0$	21.8	140	1066	1227
$p = 3\ \kappa = 0.1$	17.5	124	–	–
$p = 3\ \kappa = -0.1$	26.5	158	806	991
$p = 5\ \kappa = 0$	43.6	197.5	719	960
$p = 7\ \kappa = 0$	59.9	241.3	664	965

$$\dot{x}^{[3]}(0) = e_3\dot{q}_3(0) \Leftrightarrow$$
$$\dot{x}^3(0) = \begin{bmatrix} 0.591 \\ -0.737 \\ 0.328 \end{bmatrix} \cdot 0.0591 = \begin{bmatrix} 0.0349 \\ -0.0436 \\ 0.0194 \end{bmatrix} \tag{41}$$

Now there is an initial condition on x_2, although artificial, $\dot{x}_2^{[3]}(0) = -0.0436$, and the absorber can be tuned according to (27). Table 4 shows the numerical value of k_p. With the tuned MDOF system, 4 numerical simulations are now performed. First, all three hypothetical single-mode vibrations are actually simulated with initial conditions, respectively, being $\dot{x}^{[3]}(0)$, $\dot{x}^{[2]}(0)$ and $\dot{x}^{[1]}(0)$, for which the pumping time is found in Table 5. These measures are determined before any simulation and suggest the lower the mode, the slower the TET. Table 6 reports the TET parameters. It can be seen that the initial values of the dimensionless energies $Z_0(0)$ are much higher than the threshold values Z_0^+ for both modes 1 and 2. The more the initial energies exceeds the threshold value, the longer TET takes. Also note that ξ_{na}, although chosen as 0.1 for tuning the NES for mode 3, increases as the frequency of each mode decreases as $\xi_{na} = \frac{c_{na}}{m_{na}\omega_i}$ not only depends on the actual damping constant c_{na} and mass m_{na}, but on the modal frequency as well.

For each single-mode simulation, Fig. 14 shows its expected behavior and corresponding pumping time

Table 6 TET parameters for each mode. In all cases, tuning is done on mode 3. However for the other modes, the threshold values and xi_{na} and κ change and have significant effect on TET performance

p & κ	$Z^+_{0,m3}$	$Z^+_{0,m2}$	$Z^+_{0,m1}$	$Z_{0,m3}(0)$	$Z_{0,m2}(0)$	$Z_{0,m1}(0)$	κ_{m3}	κ_{m2}	κ_{m1}	ξ_{m3}	ξ_{m2}	ξ_{m3}
$p=3\ \kappa=0$	0.2020	0.2070	0.2803	0.2222	0.2984	11.8282	0	0	0	0.1	0.1445	0.4049
$p=3\ \kappa=0.1$	0.1480	0.1054	–	0.1628	0.2187	8.6680	0.1	0.2088	1.6394	0.1	0.1445	0.4049
$p=3\ \kappa=-0.1$	0.2678	0.3603	3.9277	0.2946	0.3956	15.6825	−0.1	−0.2088	−1.6394	0.1	0.1445	0.4049
$p=5\ \kappa=0$	0.3677	0.3739	0.4595	0.3857	0.3584	5.0702	0	0	0	0.1	0.1445	0.4049
$p=7\ \kappa=0$	0.4761	0.4831	0.5777	0.4914	0.4039	4.0535	0	0	0	0.1	0.1445	0.4049

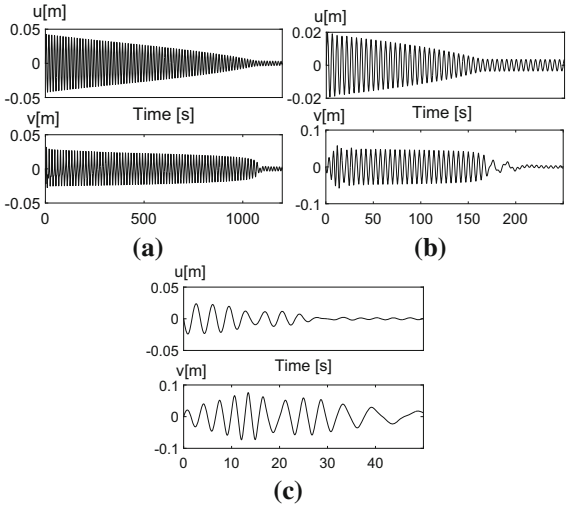

Fig. 14 The hypothetical single mode of MDOF system Fig. 13, first mode (**a**), second mode (**b**) and third mode (**c**), with the upper plot the linear mode and lower the relative nonlinear mode

found in Table 5. These simulations are not different from those performed in Sect. 6, even though those simulations are performed on an SDOF system. This is because the MDOF system considered here is only excited in a single mode, with now $u = x_2 + \varepsilon x_{na}$ and $v = x_2 - x_{na}$.

Next, the actual multi-modal system is simulated with $\dot{x}_1(0) = 0.1$, and is compared to each single-mode system. The novelty of this section are multi-modal vibrations on which the cascading time hypothesis is tested, presented in Fig. 15. From these figures, it is seen that the NES vibration, Fig. 15a, is indeed *cascading* from mode 3 to mode 1, of which the duration and magnitude corresponds to the each individual hypothetical single-mode vibration , Fig. 14. It is as if we take relative NES displacement v from Fig. 14c, then after TET of mode 3, paste the v from 14b, and this TET paste the v 14a. This sequential behavior can be formulated with the Heaviside function $\mathbb{H}(t)$:

$$x_{na} = x_{na}^{[3]} \cdot \mathbb{H}(t) + x_{na}^{[2]} \cdot \mathbb{H}\left(t - T_{\text{pump},3}\frac{\omega_3}{2\pi}\right) + x_{na}^{[1]} \cdot \mathbb{H}\left(t - T_{\text{pump},2}\frac{\omega_2}{2\pi}\right) \tag{42}$$

This sequential absorption of modes is best seen on the wavelet transform of the NES vibrations, Fig .15b, c where the TET of each mode does indeed take the beforehand computed pumping time. To asses the vibrations of the main system, the attachment point vibrations x_2 is plotted as shown in Fig. 15d. A steady decline of vibration levels is observed until TET has ceded for mode 1, after which vibrations decrease significantly slower than before.

The sum of the pumping times, Table 5, does indeed correspond to the total cascading time, the total time where the NES is active and reduces vibrations in the main system significantly. Although the time it takes to dissipate all modes seems long, up to 1000 s, note that the system has slow eigenfrequencies and that a single *linear* absorber would only dissipate the third mode while the other modes are absorbed a lot slower than the case of a single *nonlinear* absorber. See [2] for a comparison of a linear and nonlinear absorber for multi-modal vibration damping.

To summarize, the following observations were made from the simulation

- For any initial conditions on an MDOF system, hypothetical single-mode vibrations can be constructed through a modal decomposition of the initial conditions, which allow single-mode NES tuning, which provide a T_{pump} and E_{TET} and show a typical single-mode TET when the hypothetical single-mode vibrations are simulated.
- Simulating the system with the actual initial conditions shows that the NES vibrates initially only

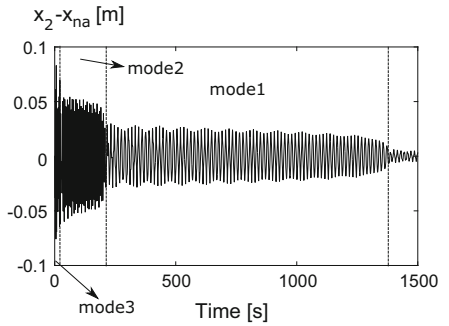

(a)

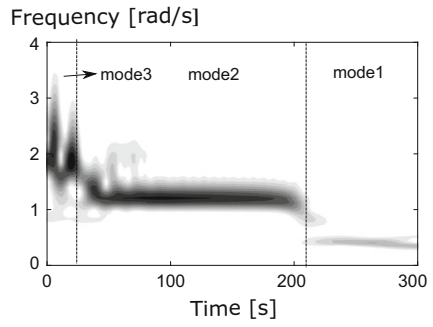

(b)

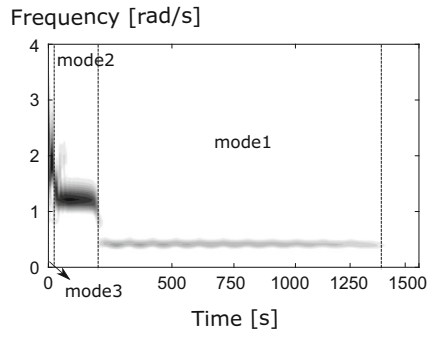

(c)

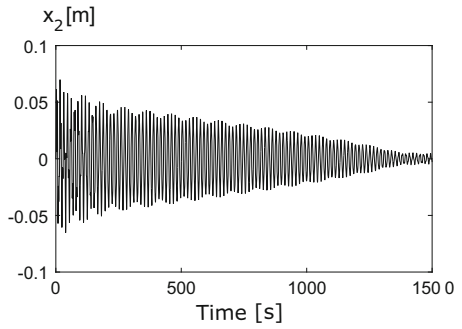

(d)

Fig. 15 The actual numerical simulation of compound system Fig. 13, with **a** the relative NES vibration v, **b**, **c** the wavelet transform of (**a**) and (**d**) the vibrations of the attachment point x_2 for $p = 3$

with the tuned mode i. The NES vibrates with this frequency ω_i for as long as the hypothetical single-mode T_{pump} and also with same magnitude. Then the NES cascades to mode $i-1$, vibrates for $T_{\text{pump},-1}$ with frequency ω_{i-1}, after which the NES cascades for mode $i-2$ and so on.

- It can be observed that the total cascading time T_{cascade} can be approximated with the sum of each individual pumping time T_{pump} of each mode that participates in the cascade, conforming the hypothesis of the total cascading time (38).
- For the whole duration of the cascading time T_{cascade}, the vibrations in the main system are steadily absorbed, mode after mode. After this duration, the vibrations have decreased significantly, and are only very slowly reduced.

The influence of p and κ on T_{pump} for single modes has been discussed in Sect. 5 and 6. Next, their influence on the cascading time will be investigated. For each parameter combination, the NES is tuned for the third mode, the cascading time will be calculated first, after which numerical simulations are performed on the actual MDOF system to verify the cascading performance. Only the wavelet transforms of the NES vibrations and the vibration of the attachment point x_2 will be presented. The pumping/cascading time will still be computed by decomposition of initial conditions.

7.4 Influence of power p

Increasing the power p increased the pumping time in the single-modal case. Here, it is investigated what influence it has on the cascading time. The pumping and cascading times for a NES tuned to the third mode with $p = 5$ and 7, for the same initial conditions (40), can be found in Table 5. As the NES is tuned for the single-modal case of mode 3, the pumping time increases, just like the single-mode case in Sect. 6. While the pumping time of the third mode for $p = 5$ doubles compared to the $p = 3$ case, for the second mode, the pumping time increases only by about 41 %. Most remarkable, however, is the 32 % decrease in the pumping time of the first mode. As mode 1 has the biggest contribution in the total cascading time, the cascading time also significantly decreases, resulting in a more performant RCC.

The numerical simulation confirms this decrease in cascading time, see the wavelet transform of Fig. 16b

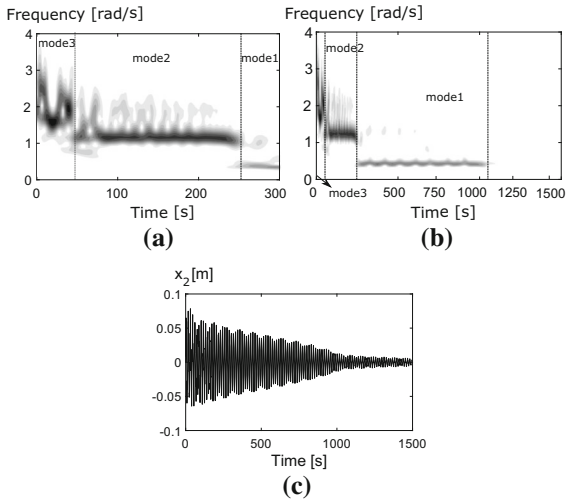

Fig. 16 The actual numerical simulation of compound system Fig. 13, with **a**, **b** the wavelet transform of the relative NES vibration v and **c** the vibrations of the attachment point x_2 for $p = 5$

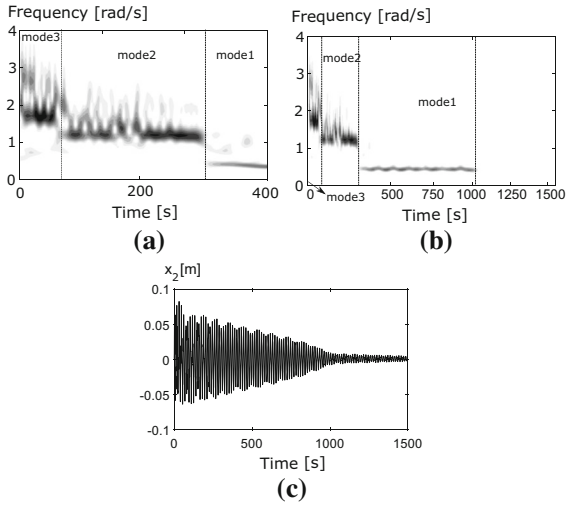

Fig. 17 The actual numerical simulation of compound system Fig. 13, with **a**, **b** the wavelet transform of the relative NES vibration v and **c** the vibrations of the attachment point x_2 for $p = 7$

for $p = 5$ and Fig. 17b for $p = 7$ compared to the wavelet transform of $p = 3$, Fig. 15c. The vibration of x_2, Figs. 16c and 17c, decrease a lot faster than for $p = 3$; Fig. 15d.

To explain the decrease in pumping time for mode 1, the SIM in E_0 and E_{na} is shown for the different modes and powers, Fig. 18. It can be seen that for the tuned mode, 3, $E_0^+ = E_0(0)$ is always the same, as it is tuned

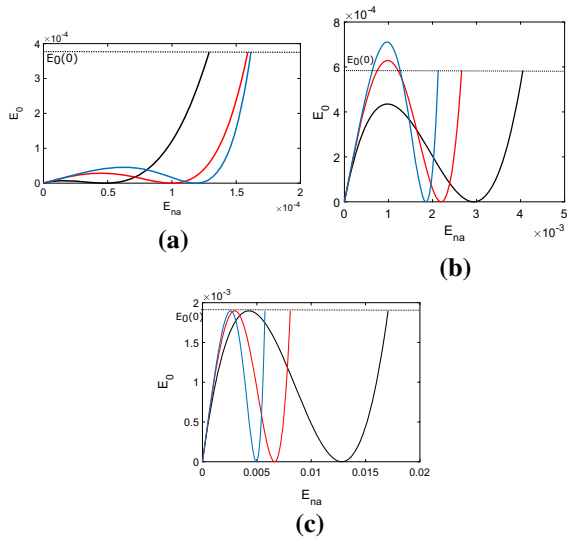

Fig. 18 The (nondimensionless) SIMs for **a** mode 1, **b** mode2 and **c** mode 3, for $p = 3$ (black), $p = 5$ (red) and $p = 7$ (blue). (Color figure online)

to this mode. This way, the TET for mode 3 is always as fast as possible for any p, Fig. 18c. However, for mode 2, the peak of the curve , E_0^+, begins to increase slightly, Fig. 18b, while it dramatically increases for mode 1, Fig. 18a, if p is increased. As E_0^+ gets closer toward $E_0(0)$, this can potentially expedite TET, as it is more optimal. However as seen in the single-mode case, this optimal TET is slower for higher p. The net result of this expediting and impeding effect still increases the pumping for mode 2. For mode 1, the expediting effect gets the upper hand in the net result.

What follows next, is a proof that E_0^+ will increase for increasing powers p, but only for the modes lower than the tuned mode.

For fixed initial condition, the initial energy of each mode of a main system $E_{0,k}(0), k \in 1, ..., n$ is a given constant, calculated from the modal initial conditions (36). The NES is designed for a mode ω_i. The mode indexes correspond to increasing frequency, $\omega_1 < \omega_2 < ... < \omega_n$. The dimensionless nonlinearity Ω of power p is tuned so that the initial energy of mode i, $E_{0,i}(0)$ corresponds with the threshold of the dimensionless energy, $Z_{0,i}^+$

$$Z_{0,i}^+ = \Omega^{\frac{2}{p-1}} E_{0,i}^+ = \frac{\alpha_p^{\frac{2}{p-1}}}{\omega_i^{2\frac{p+1}{p-1}}} E_{0,i}^+ = \frac{\alpha_p^{\frac{2}{p-1}}}{\omega_i^{2\frac{p+1}{p-1}}} E_{0,i}(0) \tag{43}$$

with $E^+_{0,i}$ the energy corresponding to the threshold, which for mode i equals $E_{0,i}(0)$, as it is this mode we tune toward. From (43), the NES is tuned, and the nonlinear coefficient α_p follows.

For mode $i-1$ the threshold is expressed as follows:

$$Z^+_{0,i-1} = \frac{\alpha_p^{\frac{2}{p-1}}}{\omega_{i-1}^{2\frac{p+1}{p-1}}} E^+_{0,i-1} \tag{44}$$

Here $E^+_{0,i-1}$ depends on p, the mode i and α_p, and does not equal $E_{0,i-1}(0)$. The ratio of (43) and (44) is:

$$\frac{E^+_{0,i-1}}{E_{0,i}(0)} \frac{\omega_i^{2\frac{p+1}{p-1}}}{\omega_{i-1}^{2\frac{p+1}{p-1}}} = \frac{Z^+_{0,i-1}}{Z^+_{0,i}} = 1 \tag{45}$$

with $\frac{Z^+_{0,i-1}}{Z^+_{0,i}} = 1$ holding if $\xi_{na} \ll 1 - \frac{\binom{p}{\frac{p-1}{2}}}{2^{p-1}} Z_{na}^{\frac{p-1}{2}}$ and $\kappa = 0$, see the SIM formula (25). To make the exponents in (45) more manageable, the natural logarithm is taken on both sides:

$$ln(E^+_{0,i-1}) = ln(E_{0,i}(0)) + 2\frac{p+1}{p-1} ln\left(\frac{\omega_{i-1}}{\omega_i}\right) \tag{46}$$

If $E^+_{0,i-1}$ increases, so will its logarithm, as the natural logarithm is a monotonically increasing function. Deriving with respect to the power p yields:

$$\frac{\partial ln(E^+_{0,i-1})}{\partial p} = \cancelto{0}{\frac{\partial ln(E_{0,i}(0))}{\partial p}} - \frac{4p}{(p-1)^2} ln\left(\frac{\omega_{i-1}}{\omega_i}\right) \tag{47}$$

with $E_{0,i}(0)$ constant, as the initial conditions stay the same.

As $ln(\frac{\omega_{i-1}}{\omega_i}) < 0$, the expression (47) is always positive. This means that for increasing powers, the energy threshold $E^+_{0,i-1}$ increases. For modes lower than ω_{i-1}, this increase is even more pronounced as the fraction $\frac{\omega_{i-2}}{\omega_i}$, $\frac{\omega_{i-3}}{\omega_i}$, …gets smaller and smaller.

As p increases, the term $\frac{4p}{(p-1)^2}$ diminishes, so will the increase of $E^+_{0,i-1}$ diminish in function of p. As $E^+_{0,i-1}$ increases for p, while $E_{0,i-1}(0)$ is constant, these two energies come closer. This way, the TET of mode $i-1$ is potentially expedited, as the closer $E_{0,i-1}(0)$ to $E^+_{0,i-1}$, the more optimal and therefore faster the TET will be. Increasing the power p will still have an impeding effect on TET, with a net result possibly being an increased or decreased T_{pump}, as seen in the above simulation. However the lower the frequency of the mode, the more likely T_{pump} is decreased. There are diminishing returns as the cascading time of $p = 7$ is already slightly higher than $p = 5$.

To summarize:

- Tuning a NES for $p > 3$ increases T_{pump} for the tuned mode, as expected from the single-mode case. However, T_{pump} of the other modes seems to either increase less significantly or even decreases. This can result in an actual decrease T_{cascade} for $p > 3$ compared to $p = 3$.
- Numerical simulations confirmed this. In total, the cascading time decreased and the vibrations of the main system are absorbed faster.
- It was shown that for modes lower than the tuned mode i, the threshold energy E^+_0 increases for increasing p getting closer and closer to $E_0(0)$
- The net result of the expediting effect of increased E^+_0 and the impeding effect of increased p can either be an increase of decrease in pumping time. The lower the mode frequency, the more the expediting effect gets the upper hand.

7.5 Influence of linear part κ

In the single-mode case, a $\kappa > 0$ decreased T_{pump} while $\kappa < 0$ caused an increase. Here it is investigated whether there also is an expediting effect for modes lower than the tuned one in the multi-modal case. As with the dimensionless damping ξ_{na}, κ also depends on ω_i, $\kappa = \frac{k_{\text{lin}}}{m_{na}\omega_i^2}$. A proposed κ is associated with the mode which is used to tune the NES. For the modes below the tuned mode, κ will increase in magnitude. For $\kappa > 0$, this could lead to the condition for TET (23), $\kappa < 1$, not being met.

The pumping and cascading time are calculated for $p = 3$ and $\kappa = 0.1$ & -0.1, Table 5. Keep in mind that although the NES is tuned for mode 3, to calculate T_{pump} for mode 2 and 1, the $\kappa \neq 0.1$ or -0.1, see Table 3 for their values. $\kappa = 0.1$ for mode 3 corresponds to $\kappa = 1.6394$ for the first mode, which means the condition for TET (23) is not met ($\kappa > 1$), there is no bifurcation in the SIM so no T_{pump} can be calculated for more 1. The NES tuned with $\kappa = -0.1$ for mode 3 or $\kappa = -1.6394$ for mode 1, TET conditions are still met, $\kappa < 1$, and T_{pump} of mode 1 has even decreased compared to $\kappa = 0$. The expediting effect for $\kappa < 0$ can again be explained with the increase of E^+_0 for modes lower than the tuned ones, Fig. 21.

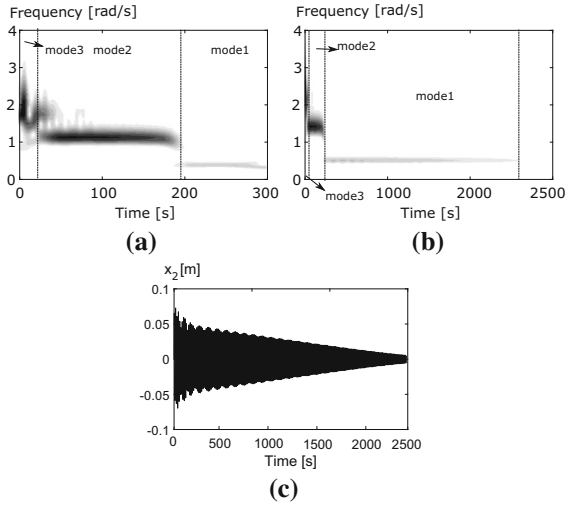

Fig. 19 The actual numerical simulation of compound system Fig. 13, with **a**, **b** the wavelet transform of the relative NES vibration v and **c** the vibrations of the attachment point x_2 for $p = 3$ and $\kappa = 0.1$

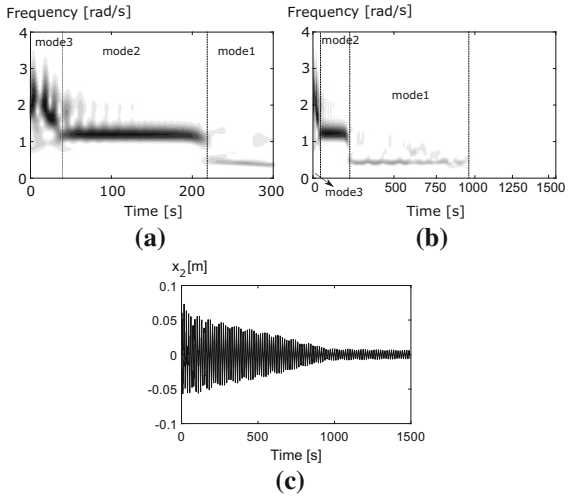

Fig. 20 The actual numerical simulation of compound system Fig. 13, with **a**, **b** the wavelet transform of the relative NES vibration v and **c** the vibrations of the attachment point x_2 for $p = 3$ and $\kappa = -0.1$

Numerical simulations show both the predicted T_{pump} and T_{cascade} as well as the absence of TET for mode 1 for $\kappa = 0.1$, Fig. 19b and Fig. 20b for $\kappa = -0.1$. The vibrations in both main system and NES dissipate much slower for $\kappa = 0.1$ after TET of mode 2, Fig. 19, than $\kappa = -0.1$, Fig. 19c. This can be explained with the SIMs shown in Fig. 20c. As E_0^+ increased enormously for mode 1, for $\kappa = -0.1$, the retarding effect associated with a negative κ is compensated. An additional advantage for negative κ is that the conditions for TET are *always* met.

- While $\kappa > 0$ decreases pumping time of the modes where TET conditions are still met, the lower the mode frequency, to more likely the TET conditions are not met and the vibrations of the modes are reduced very slowly
- For $\kappa < 0$ there is both an impeding effect ($\kappa < 0$) and an expediting effect (increasing E_0^+ for lower modes) with as a net result either an increase or decrease in pumping time. As with increasing power p, the lower frequency the mode has, the more likely a decrease in pumping time.
- Numerical results confirmed this and showed that the system's vibrations persist very long for $\kappa > 0$, as conditions for TET are not met for all modes.

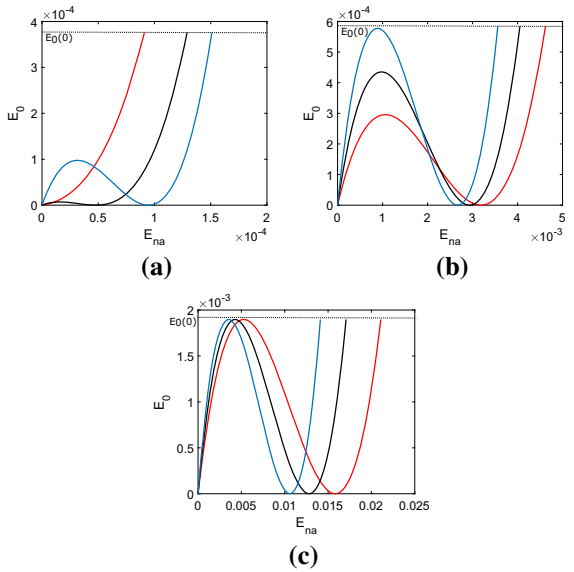

Fig. 21 The (nondimensionless) SIMs for **a** mode 1, **b** mode2 and **c** mode 3, for $\kappa = 0$ (black), $\kappa = 0.1$ (red) and $\kappa = -0.1$ (blue). (Color figure online)

8 Performance for more general mechanical systems

While deriving the SIM, and determining the pumping and cascading time, several assumptions were made. Here the influence of relaxing two of these assumptions is investigated; 1) allow modal damping to calculate

pumping and cascading time and 2) nonlinearities in the main system (up to $\mathscr{O}(\varepsilon^0)$).

8.1 Introducing modal damping

The modal damping itself does not change tuning, as it is not present in the expression of the SIM, the 2nd equation in (21). It will however increase dissipation and thus expedite TET. No modal damping was introduced to easily solve (30):

$$\frac{1}{\omega_i}\frac{\partial Z_{na}}{\partial T_1} = \frac{-\xi_{na} Z_{na} - \xi Z_0}{\frac{p\left(\frac{p}{\frac{p-1}{2}}\right)^2}{2^{2(p-1)}} Z_{na}^{p-1} - (1-\kappa)\frac{(p+1)\left(\frac{p}{\frac{p-1}{2}}\right)}{2^{p-1}} Z_{na}^{\frac{p-1}{2}} + (1-\kappa)^2 + \xi_{na}^2} \tag{48}$$

When the modal damping $\xi = 0$, separation of variables is simple and subsequent integrating result in the pumping time. Here, an expression for the pumping time with modal damping is sought. Trying to separate the variables and dividing both sides by Z_{na} yields:

$$\left(-\xi_{na} - \xi\frac{Z_0}{Z_{na}}\right)\partial T_1 \omega_i = \Big(\frac{p\left(\frac{p}{\frac{p-1}{2}}\right)^2}{2^{2(p-1)}} Z_{na}^{p-2} - (1-\kappa)\frac{(p+1)\left(\frac{p}{\frac{p-1}{2}}\right)}{2^{p-1}} Z_{na}^{\frac{p-3}{2}} + \frac{(1-\kappa)^2 + \xi_{na}^2}{Z_{na}}\Big)\partial Z_{na} \tag{49}$$

The right side entirely depends on Z_{na}, but on the left, the term $\frac{Z_0}{Z_{na}}$ prevents complete separation of variables. Consider only the left part of (49), where the SIM relation,2nd equation of (21), removes Z_0:

$$\begin{aligned}&\left(-\xi_{na} - \xi\left[\xi_{na}^2 + \left(1-\kappa - \frac{\left(\frac{p}{\frac{p-1}{2}}\right)}{2^{p-1}} Z_{na}^{\frac{p-1}{2}}\right)^2\right]\right)\partial T_1\omega_i \\ &= \left(-\xi_{na} - \xi\xi_{na}^2 - \xi(1-\kappa)^2\right)\partial T_1\omega_i \\ &\quad - \xi\left(\frac{\left(\frac{p}{\frac{p-1}{2}}\right)^2}{2^{2(p-1)}} Z_{na}^{p-1} - 2(1-\kappa)\frac{\left(\frac{p}{\frac{p-1}{2}}\right)}{2^{p-1}} Z_{na}^{\frac{p-1}{2}}\right)\partial T_1\omega_i\end{aligned} \tag{50}$$

Although there is no complete separation of variables, as $Z_{na}(T_1)$, both sides of (49) are integrated anyway

$$\begin{aligned}&\left(-\xi_{na} - \xi\xi_{na}^2 - \xi(1-\kappa)^2\right) T_1\omega_i \\ &-\xi\omega_i\int_0^{T_1}\left(\frac{\left(\frac{p}{\frac{p-1}{2}}\right)^2}{2^{2(p-1)}} Z_{na}^{p-1} - 2(1-\kappa)\frac{\left(\frac{p}{\frac{p-1}{2}}\right)}{2^{p-1}} Z_{na}^{\frac{p-1}{2}}\right)\partial T_1 \\ &= I_Z(Z_{na}) + \mathscr{C}\end{aligned} \tag{51}$$

with $\mathscr{C}$ the constant of integration and

$$\begin{aligned}I_Z(Z_{na}) = &\frac{p\left(\frac{p}{\frac{p-1}{2}}\right)^2}{(p-1)2^{2(p-1)}} Z_{na}^{p-1} \\ &- \frac{\left(\frac{p}{\frac{p-1}{2}}\right)(1-\kappa)(p+1)}{\frac{p-1}{2}2^{p-1}} Z_{na}^{\frac{p-1}{2}} \\ &+ \left((1-\kappa)^2 + \xi_{na}^2\right) ln(Z_{na})\end{aligned} \tag{52}$$

The slow time T_1 between the two states $Z_{na,1}$ and $Z_{na,2}$ on the SIM is

$$\begin{aligned}&\left(-\xi_{na} - \xi\xi_{na}^2 - \xi(1-\kappa)^2\right) T_1\omega_i \\ &-\xi\omega_i\int_0^{T_1}\left(\frac{\left(\frac{p}{\frac{p-1}{2}}\right)^2}{2^{2(p-1)}} Z_{na}^{p-1} - 2(1-\kappa)\frac{\left(\frac{p}{\frac{p-1}{2}}\right)}{2^{p-1}} Z_{na}^{\frac{p-1}{2}}\right)\partial T_1 \\ &= I_Z(Z_{na,1}) - I_Z(Z_{na,1})\end{aligned} \tag{53}$$

To be able to solve the integral on the left-side equation, either the function $Z_{na}(t)$ has to be derived from the slow flow dynamics, or a constant Z_{na} is assumed. Here it is opted for the latter. This constant Z_{na} is only assumed to solve the unsolvable integral, not for the whole equation. During TET, the energy Z_{na} in slow flow looks almost constant, see Fig. 11 for simulations of an undamped main system, where the dashed lined seem almost constant during TET. See Fig. 22 which shows Z_{na} for $p = 3$ of this simulation. Only a small error would be introduced by assuming $Z_{na}(t) = Z_{na,c}$, with $Z_{na,c}$ a constant. Finally, the time between the two energy states, now chosen as $Z_{na}(0)$ and Z_{na}^+, is:

$$\begin{aligned}&\Big(-\xi_{na} - \xi\xi_{na}^2 - \xi(1-\kappa)^2 + \xi\left(\frac{\left(\frac{p}{\frac{p-1}{2}}\right)^2}{2^{2(p-1)}} Z_{na,c}^{p-1}\right. \\ &\left.-2(1-\kappa)\frac{\left(\frac{p}{\frac{p-1}{2}}\right)}{2^{p-1}} Z_{na,c}^{\frac{p-1}{2}}\right)\Big) T_{\text{pump}} 2\pi \\ &= I_Z(Z_{na,1}) - I_Z(Z_{na,2})\end{aligned} \tag{54}$$

from which the pumping time T_{pump} follows. Here, a $Z_{na,c}$ is estimated through the undamped simulations,

Table 7 Numerical values for SDOF system, Fig. 8. Other numeric values are found on Table 1

Parameter	Value
$c\ [\frac{Ns}{m}]$	0.01
$Z_{na,c}\ [-]$	1.63
$T_{\text{pump}}\ \frac{\omega_i}{2\pi}\ [s]$	63.9
$T_{\text{pump},c=0.01}\ \frac{\omega_i}{2\pi}\ [s]$	50.0

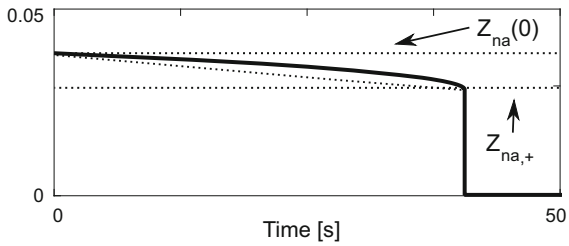

Fig. 22 Undamped slow flow simulation for p=3 taken from Fig. 11, illustrating the slow change of Z_{na} from its initial value

e.g., Fig. 22, as the average function value of Z_{na} during TET:

$$Z_{na,c} = \frac{1}{T_{\text{pump}}} \int_0^{T_{\text{pump}}} Z_{na}(t)dt \tag{55}$$

8.1.1 SDOF example

To show the viability of the proposed method, the simulations performed earlier on an SDOF system for $p = 3$ and $\kappa = 0$, in Sect. 6, are repeated with added damping of c = 0.01 $\frac{\text{Nm}}{\text{s}}$. The nonlinear coefficient of the NES is not altered as modal damping does not affect tuning. The pumping time for both damped and undamped are found in Table 7. $Z_{na,c}$ was determined as the average function value of Figure 22. The predicted value of T_{pump} in the damped case, 50 s, is in accordance to both observed pumping time, in the slow flow simulation and the actual, fast, dynamics, Fig. 23.

8.1.2 MDOF example

The cascading time was determined by assuming that the initial energy of modes lower than tuned mode i, is kept inside the main system, until this mode engages in RCC. With the addition of modal damping, the energy of the modes not active in the RCC will not be preserved but dissipated by this modal damping. The dynamics for a mode k not active in RCC can be seen as only

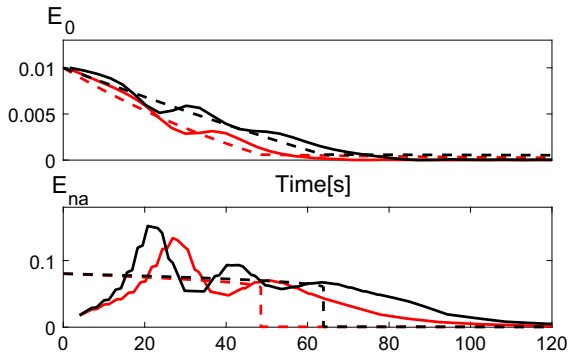

Fig. 23 TET in a damped system (red) and undamped (black). (Color figure online)

changing in $Z_{0,k}$ while $Z_{na,k} = 0$. Solving (21) for $Z_{na,k} = 0$:

$$Z_{0,k}(T_1) = Z_{0,k}(0)e^{-\lambda T_1} \tag{56}$$

with $Z_{0,k}(0)$ determined by the modal decomposition of the initial conditions. If the cascade was initiated at mode i, then when it is the turn of mode k to start in the cascade, the energy in mode k will be reduced to $Z_{0,k}(T_{1,\text{start},k})$ by (56) for a time:

$$T_{1,\text{start},k} = \varepsilon_k \sum_{l=0}^{i-k-1} T_{\text{pump},i-l} \cdot \frac{\omega_{i-l}}{2\pi} \tag{57}$$

being the sum of the pumping times of the previous modes who were in the RCC, with $\varepsilon_k = \frac{1}{m_{na}e_k(\ell)^2}$ different for each mode. It is the $Z_{0,k}(T_{1,\text{start},k})$ that is used to calculate the initial $Z_{na,k}$ required to calculate the pumping time for mode k. A simulation is performed on the system presented in Sect. 7 for $p = 3$ and $\kappa = 0$. The cascading time for the damped system is almost halved compared to the undamped case, Table 8. Note that to determine the constant $Z_{na,c}$ for calculating the pumping of each mode, single-mode simulation of the slow flow need to be performed first, by applying the modal decomposition of the initial conditions. Damping has the most effect on the first mode, as this mode stays the longest in the system. The numerical simulation of the undamped system are shown in Fig. 15. The damped case is shown in Fig. 24 and reveal the energy is mitigated a lot faster and that the cascading time of the damped system is estimated well.

Table 8 Pumping time for each mode and the cascade time damped vs undamped

	$T_{\text{pump},3}\frac{\omega_3}{2\pi}$	$T_{\text{pump},2}\frac{\omega_2}{2\pi}$	$T_{\text{pump},1}\frac{\omega_1}{2\pi}$	T_{cascade}
$p=3\ \kappa=0\ c=0$	21.8	140	1066	1227
$p=3\ \kappa=0\ c=0.01$	16.3	112	609	738

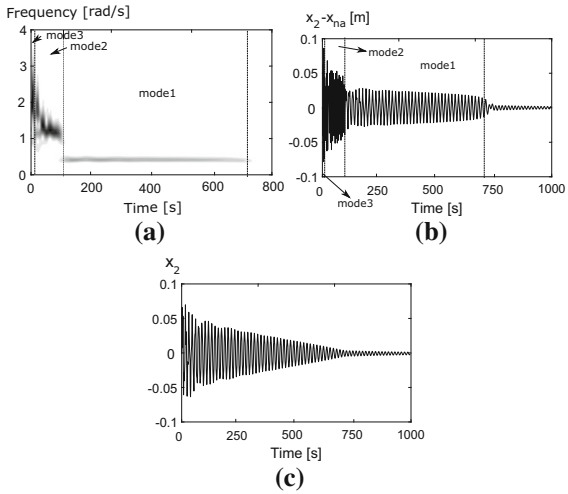

Fig. 24 The actual numerical simulation of compound system Fig. 13, with (a) the wavelet transform of the relative NES vibration v, (b) the displacement of the relative NES vibration and (c) the vibrations of the attachment point x_2 for $p=3, \kappa=0$ and $c=0.01$

8.2 Additional nonlinearity in main system

The same procedure to calculate the SIM and slow flow dynamics can be applied to a main system which has an additional nonlinearity somewhere. It is assumed that the nonlinearity is an nonlinear stiffness of uneven power p_m, and the main system is linearizable so that it has linear eigenfrequencies. Assuming that the system still vibrates according to a single mode, a mode of the linearized main system, an added nonlinearity will be found in (9) as:

$$\begin{aligned}&\ddot{x}_\ell+\varepsilon\lambda\dot{x}_\ell+\omega_i^2x_\ell+\beta_{p_m}x_\ell^{p_m}+\varepsilon\ddot{x}_{na}=0\\&\varepsilon\ddot{x}_{na}+\varepsilon\lambda_{na}(\dot{x}_{na}-\dot{x}_\ell)+\varepsilon\alpha_p(x_{na}-x_\ell)^p\\&\quad+\varepsilon\kappa\omega_i^2(x_{na}-x_\ell)=0\end{aligned}\tag{58}$$

Depending on the order of the coefficient β_{p_m}, $\mathcal{O}(\varepsilon^1)$ or $\mathcal{O}(\varepsilon^0)$, it will appear differently in the slow flow dynamics. Note that no discussion will be held for purely nonlinear main systems, the nonlinearity here is seen as a deviation of the linearized system. In introduction to vibration absorbers for purely nonlinear main systems is found in [19].

8.2.1 β_{p_m} of $\mathcal{O}(\varepsilon^1)$

After some calculation the nonlinearity will appear in the second equation of (17) proportional to φ_0 with $B=\frac{\beta_{p_m}}{\omega_i^{p_m+1}}$

$$\begin{aligned}&\frac{\partial\varphi_0}{\partial T_1}+\frac{\partial\varphi_1}{\partial T_0}+\frac{\lambda\varphi_0}{2}+\frac{\omega_i^2\varphi_{na0}}{2i\omega_i}-\frac{\omega_i^2\varphi_0}{2i\omega_i}-\\&i\frac{B\omega_i}{(2)^{p_m}}\binom{p_m}{\frac{p_m-1}{2}}|\varphi_0|^{p_m-1}\varphi_0=0\end{aligned}\tag{59}$$

It will then appear only in the second equation of (19), in the phasing of the slow flow dynamics:

$$\begin{aligned}\frac{R_0}{\omega_i}\frac{\partial\delta_0}{\partial T_1}=&-\frac{R_0}{2}+\frac{cos(\delta_{na}-\delta_0)}{2}R_{na}\\&-\frac{B}{2\omega_i}\binom{p_m}{\frac{p_m-1}{2}}R_0^p\end{aligned}\tag{60}$$

The nonlinearity will influence the phase of the slow flow dynamics. In further derivations, this second equation of (19) is not used in following derivations, an identical expression for the SIM and slow flow dynamics (21) is found for β_{p_m} of $\mathcal{O}(\varepsilon^1)$. The tuning procedure, pumping time and cascading time are therefore not altered by the nonlinearity of $\mathcal{O}(\varepsilon^1)$ in the main system, and so is robust against these nonlinearities. There only is a difference in phasing on slow time scale T_1. A simulation is performed as an illustration. The SDOF system in Sect. 6 is taken for $p=3$ and $\kappa=0$, but with an additional nonlinear stiffness from main mass to ground, $0.5x^3$, with the coefficient of $\mathcal{O}(\varepsilon^1)$ ($\varepsilon=0.02$). The NES vibration, Fig 25b, and main mass vibration, Fig 25a, both in red dash, are almost identical as if no nonlinearity is present (in black). The effect on phasing on the slow time is not seen.

8.2.2 β_{p_m} of $\mathcal{O}(\varepsilon^0)$

The nonlinearity of order $\mathcal{O}(\varepsilon^0)$ will appear in (17) in the first two equations:

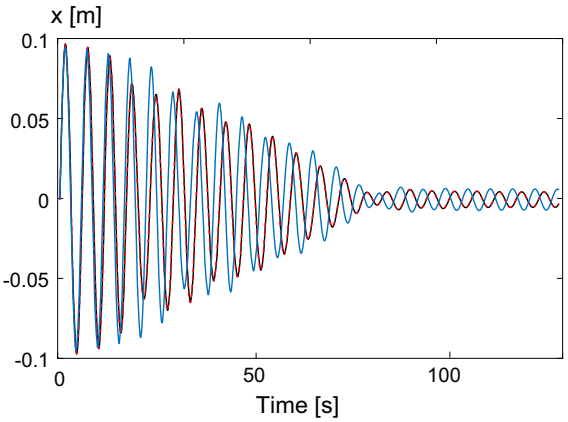

(a)

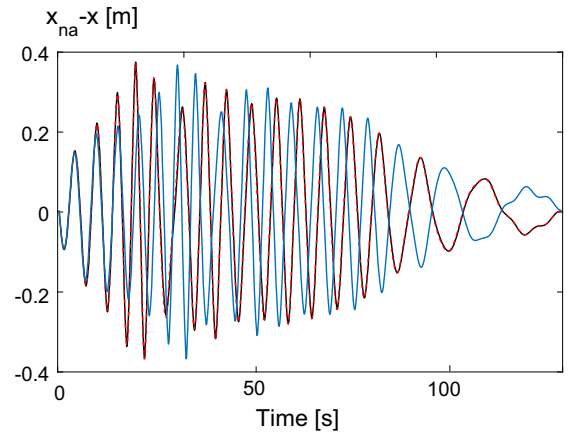

(b)

Fig. 25 Numerical simulation of system Fig. 8 for $\dot{x}(0) = 0.1$, $p = 3$ and $\xi_{na} = 0.1$. Main system vibration (a) and NES (b) for linear main system (black), with additional nonlinear spring $0.5x^3$ (red) and $10x^3$ (blue). (Color figure online)

$$\frac{\partial \varphi_0}{\partial T_0} = i\frac{B}{(2)^{p_m}}\binom{p_m}{\frac{p_m-1}{2}}|\varphi_0|^{p_m-1}\varphi_0\frac{\partial \varphi_0}{\partial T_1} + \frac{\partial \varphi_1}{\partial T_0} + \frac{\lambda\varphi_0}{2} + \frac{\omega_i^2\varphi_{na0}}{2i\omega_i} - \frac{\omega_i^2\varphi_0}{2i\omega_i} - i\cdot\frac{B\omega_i}{(2)^p}f(\varphi_{na0},\bar{\varphi}_{na0},\varphi_0,\bar{\varphi}_0,\varphi_1,\bar{\varphi}_1) = 0 \tag{61}$$

which hints in the first equation that this nonlinearity has influence on a fast time scale. However, rewriting the complex variable φ_0 in polar notation for time scale T_0, $\varphi_0 = R_0(T_0)e^{i\delta_0(T_0)}$, and splitting in real and imaginary part yields:

$$\frac{\partial R_0(T_0)}{\partial T_0} = 0$$

$$\frac{R_0(T_0)}{\omega_i}\frac{\partial \delta_0(T_0)}{\partial T_0} = -\frac{\beta_p}{2\omega_i}\binom{p}{\frac{p-1}{2}}R_0^p \tag{62}$$

which reveals that just like for $\mathcal{O}(\varepsilon^1)$, the amplitude is not effected, but only the phase. This time in the fast time scale instead of the slow.

In the second equation in (61), the nonlinearity will cause a coupling between φ_0 and φ_{na0}, lumped in $f(\cdot) \in \mathbb{R}$. This term is multiplied by the imaginary unit, i, which will cause it to appear in the phase dynamics of the slow flow, the second equation of (19). This way again only the slow phase dynamics are altered and not the amplitude. As in previous section, this does not alter the slow flow dynamics and SIM, (21). The derivations of tuning and performance measures are thus robust against additional nonlinearities in the main system of $\mathcal{O}(\varepsilon^1)$ and $\mathcal{O}(\varepsilon^0)$. To illustrate this for $\mathcal{O}(\varepsilon^0)$, the same system is taken as before, but now with the nonlinearity $10x^3$, with the coefficient of $\mathcal{O}(\varepsilon^0)$. The NES vibration, Fig 25b, and main mass vibration, Fig 25a, both in blue, are of the same magnitude but shift in phase over time compared to the linear main system (in black). The only effect of the nonlinearity is on the phase on the fast time scale, just as predicted.

9 Conclusion

In this study, the tuning and performance of a NES for absorbing excessive vibration with TET in a mechanical system was thoroughly investigated, both single-mode and multi-modal vibrations. A more application-oriented approach was taken than typically done in existing literature. Central in this approach is the derived slow invariant manifold, a static relation which describes the energy exchange on a slow time scale. First, tuning formulas for a NES for single-modal vibrations were established. The connecting stiffness of the NES can have any uneven power and a small positive or negative linear part. Then, the algebraic performance measures pumping time and energy dissipation were defined, which required no numerical simulation to be determined. This way, the influence of different powers and linear part of the NES's connecting stiffness on TET performance can be quickly assessed. For the single-mode case, increasing the power and negative linear part impeded TET while a positive linear part expedited TET. Numerical simulations, although not required to asses the TET performance, confirmed the merit of both the pumping time and dissipated

energy. Next, tuning rules were established for multi-modal frequency absorption capability (RCC) of a single NES. These rules are based on the single-mode case by decomposing of initial conditions on the main system into single modes. Similar to the single-modal case, a novel algebraic performance measure for the speed RCC was defined, the cascading time, the time the NES takes to dissipate all the modes. Here, it was concluded that higher power and negative linear part actually expedited the RCC while a positive linear part impedes the RCC, opposite to the single-modal case. Numerical simulations again confirmed the validity of this cascading time.

Compliance with ethical standards

Conflict of interest The authors declare that they have no conflict of interest.

References

1. Vakakis, A.F., Gendelman, O.V., Bergman, L.A., McFarland, M.D., Kerschen, G., Lee, Y.S.: Nonlinear Targeted Energy Transfer in Mechanical and Structural Systems. Springer, Netherlands (2009)
2. Petit, F., Loccufier, M., Aeyels, D.: Feasibility of nonlinear absorbers for transient vibration reduction. In: Proceedings of ISMA 2010: International Conference on Noise and Vibration Engineering, pp. 1219–1233 (2010)
3. Lee, Y.S., Kerschen, G., Vakakis, A.F., Panagopoulus, P., Bergman, L.A., McFarland, M.D.: Complicated dynamics of a linear oscillator with a light, essentially nonlinear attachment. Phys. D Nonlinear Phenom. **204**, 41–69 (2005)
4. Kerschen, G., Lee, Y.S., Vakakis, A.F., McFarland, M.D., Bergman, L.A.: Irreversible passive energy transfer in coupled oscillators with essential nonlinearity. SIAM J. Appl. Math. **66**, 648–679 (2006)
5. Kurt, M., Slavkin, I., Eriten, M., McFarland, D., Gendelman, O., Bergman, L., Vakakis, A.: Effect of 1: 3 resonance on the steady-state dynamics of a forced strongly nonlinear oscillator with a linear light attachment. Arch. Appl. Mech. **84**(8), 1189 (2014)
6. Lin, D., Oguamanam, D.: Targeted energy transfer efficiency in a low-dimensional mechanical system with an essentially nonlinear attachment. Nonlinear Dyn. **82**(1–2), 971–986 (2015)
7. Starosvetsky, Y., Gendelman, O.: Interaction of nonlinear energy sink with a two degrees of freedom linear system: internal resonance. J. Sound Vib. **329**(10), 1836–1852 (2010)
8. Kerschen, G., Vakakis, A.F., Lee, Y.S., Mcfarland, D.M., Kowtko, J.J., Bergman, L.A.: Energy transfers in a system of two coupled oscillators with essential nonlinearity: 1: 1 resonance manifold and transient bridging orbits. Nonlinear Dyn. **42**(3), 283–303 (2005)
9. Vaurigaud, B., Savadkoohi, A.T., Lamarque, C.-H.: Targeted energy transfer with parallel nonlinear energy sinks. Part i: design theory and numerical results. Nonlinear Dyn. **66**(4), 763–780 (2011)
10. Nguyen, T.A., Pernot, S.: Design criteria for optimally tuned nonlinear energy sinks. Part 1: transient regime. Nonlinear Dyn. **69**(1–2), 1–19 (2012)
11. Petit, F., Loccufier, M., Aeyels, D.: The energy thresholds of nonlinear vibration absorbers. Nonlinear Dyn. **74**(3), 755–767 (2013)
12. Quinn, D.D., Gendelman, O., Kerschen, G., Sapsis, T.P., Bergman, L.A., Vakakis, A.F.: Efficiency of targeted energy transfers in coupled nonlinear oscillators associated with 1: 1 resonance captures: Part i. J. Sound Vib. **311**(3), 1228–1248 (2008)
13. Sapsis, T., Vakakis, A.F., Gendelman, O.V., Bergman, L.A., Kerschen, G., Quinn, D.: Efficiency of targeted energy transfers in coupled nonlinear oscillators associated with 1: 1 resonance captures: Part ii, analytical study. J.Sound Vib. **325**(1), 297–320 (2009)
14. Tripathi, A., Grover, P., Kalmár-Nagy, T.: On optimal performance of nonlinear energy sinks in multiple-degree-of-freedom systems. J.Sound Vib. **388**, 272–297 (2017)
15. Vakakis, A.F., Manevitch, L., Gendelman, O., Bergman, L.: Dynamics of linear discrete systems connected to local, essentially non-linear attachments. J.Sound Vib. **264**(3), 559–577 (2003)
16. Kerschen, G., Kowtko, J.J., McFarland, D.M., Bergman, L.A., Vakakis, A.F.: Theoretical and experimental study of multimodal targeted energy transfer in a system of coupled oscillators. Nonlinear Dyn. **47**(1), 285–309 (2007)
17. Strogatz, S.H.: Nonlinear Dynamics and Chaos: With Applications to Physics, Biology, Chemistry, and Engineering. Hachette, New York (2014)
18. Gendelman, O.V.: Bifurcations of nonlinear normal modes of linear oscillator with strongly nonlinear damped attachment. Nonlinear Dyn. **37**(2), 115–128 (2004)
19. Viuië, R., Kerschen, G.: Nonlinear vibration absorber coupled to a nonlinear primary system: a tuning methodology. J. Sound Vib. **326**(6), 780–793 (2009)